Absolute Hydration Free Energy Scale for Alkali and Halide Ions Established from Simulations with a Polarizable Force Field

Guillaume Lamoureux[†,‡] and Benoît Roux*[,§,||]

Département de physique, Université de Montréal, C.P. 6128, succ. centre-ville, Montréal, Québec H3C 3J7, Canada, and Department of Biochemistry, Weill Medical College of Cornell University, 1300 York Avenue, New York, New York 10021

Received: October 21, 2005; In Final Form: December 8, 2005

A polarizable potential function for the hydration of alkali and halide ions is developed on the basis of the recent SWM4-DP water model [Lamoureux, G.; MacKerell, A. D., Jr.; Roux, B. *J. Chem. Phys.* **2003**, *119*, 5185]. Induced polarization is incorporated using classical Drude oscillators that are treated as auxiliary dynamical degrees of freedom. The ions are represented as polarizable Lennard-Jones centers, whose parameters are optimized to reproduce the binding energies of gas-phase monohydrates and the hydration free energies in the bulk liquid. Systematic exploration of the parameters shows that the monohydrate binding energies can be consistent with a unique hydration free energy scale if the computed hydration free energies incorporate the contribution from the air/water interfacial electrostatic potential (−540 mV for SWM4-DP). The final model, which can satisfyingly reproduce both gas and bulk-phase properties, corresponds to an absolute scale in which the intrinsic hydration free energy of the proton is −247 kcal/mol.

1. Introduction

Numerous fundamental processes in chemistry and biology involve the interaction of small alkali and halide ions with water molecules. Depending on the system of interest, the physical character of ion hydration varies widely, from small clusters in the gas phase to bulk solvation in the liquid phase. One way to better understand the hydration of small ions is to use computer simulations of atomic models based on potential functions. For example, previous simulations of aqueous ionic solutions have shown that they can be a valuable tool to gain more insight about these systems.[1−7] However, for meaningful computer simulations, it is important to use potential functions that are as accurate and realistic as possible. In particular, induced polarization, which is generally neglected in biomolecular simulations, is of great concern in the case of aqueous ionic systems where nonadditive many-body effects could be very important.

In principle, accurate potential functions for computer simulations can be developed and validated by comparing to experimental data (gas phase and bulk) and to the results of high-level ab initio computations. Obviously, a central piece of information to construct valid and accurate computational models of aqueous ionic systems is the experimentally measured absolute hydration free energies of the alkali and halide series.[8−16] However, interpreting correctly the data about the absolute hydration free energies of charged species and making full use of it in constructing an accurate computational model in not as straightfoward as one might wish. One important difficulty arises from the fact that thermodynamic or electrochemical measurements involve neutral macroscopic systems and have access only to irreducible, *conventional* hydration free energies that are either the sum of the absolute free energies of an ion and a counterion, $\Delta G_{hydr}(M^+) + \Delta G_{hydr}(X^-)$, or the difference of the free energies of two ionic species of the same valence, $\Delta G_{hydr}(M_1^+) - \Delta G_{hydr}(M_2^+)$. In fact, the absolute hydration free energy of a single ion cannot be resolved from calorimetric or voltammetric experiments alone. Traditionally, absolute free energies have been estimated using an "extrathermodynamic" assumption based on an a priori notion that two specific ions of opposite charges have comparable absolute free energies. The TATB hypothesis,[13] which consists of postulating that tetraphenylarsenium (TA^+) and tetraphenylborate (TB^-) ions have the same hydration free energies, is the most commonly used. But further considerations suggest that the free energies of those ions have no reason a priori of being identical.[17]

The difficulties of the extrathermodynamic assumptions are further compounded by the fact that in a real physical system, the total reversible work to take an ion from the gas phase and transfer it into a bulk liquid phase includes a contribution from the electrostatic potential associated with the vacuum/liquid interface (the "phase potential").[18] Accordingly, in discussions of the hydration free energies of ionic species, one may consider the *real* physical value ΔG_{hydr}^{real}, which includes the contribution of the phase potential arising from crossing the physical air/water interface, and the *intrinsic* bulk phase value ΔG_{hydr}^{intr} (sometimes referred to as "absolute" free energy), which is independent of any interfacial potential. Such an electrostatic potential arises from the anisotropic orientational distribution of the solvent molecules near the interface. Direct measurements of ϕ are very difficult, and it may be necessary to resort to computer simulations to estimate its value.[19] For an ion of valence z, these values are related through the phase potential ϕ such as, $\Delta G_{hydr}^{real} = \Delta G_{hydr}^{intr} + zF\phi$ (where F is the Faraday

* To whom correspondence should be addressed. E-mail: roux@uchicago.edu.
† Université de Montréal.
‡ Current address: Center for Molecular Modeling, Department of Chemistry, University of Pennsylvania.
§ Weill Medical College of Cornell University.
|| Current address: Institute for Molecular Pediatric Sciences, Center for Integrative Studies, University of Chicago, 929 East 57th Street, Room W323B, Chicago, IL 60637.

10.1021/jp056043p CCC: $33.50
Published on Web 01/27/2006

constant, 23.06 kcal/mol/V). In simple terms, the existence of an interfacial potential ϕ implies that there is an offset contribution of $+F\phi$ kcal/mol for the real free energy of a monovalent cation and, correspondingly, of $-F\phi$ kcal/mol for the real free energy of a monovalent anion.[20] Because this contribution cancels out for neutral macroscopic systems, neither the "real" nor "intrinsic" hydration free energies can be extracted from standard measurements.

The primary goal of the present effort is to characterize the hydration of alkali and halide ions using a potential function that incorporates induced polarization. The approach used here is similar to that employed for the design of the SWM4-DP water model.[21] It is based on the classical Drude oscillator model,[22] which represents electronic induction by introducing a massless charged particle, attached to each polarizable atom by a harmonic spring. Previous work has shown that this approach is useful to model polarization in aqueous systems[23−28,21] and ion solvation.[2,5,29]

The article is organized as follows. Section 2 presents the functional form of the polarizable model for the ions. Some important methodological issues regarding the calculation of real and intrinsic hydration free energies are also discussed. Section 3 discusses the target data and the procedure by which the empirical parameters are adjusted. Section 4.2 presents an assessment of the model for small alkali and halide hydrates. Section 4.3 analyzes and discusses the hydration structure predicted by the model.

2. Model and Computational Methods

2.1. Classical Drude Polarizable Model. The ions are represented as point charges of $\pm|e|$ embedded at the center of a Lennard-Jones "6−12" interaction with the oxygen atoms of the water molecules. Their electronic polarizability is modeled via a classical Drude oscillator attached to the nucleus.[28] The water molecules are represented using the recently developed SWM4-DP polarizable water model.[21] The SWM4-DP potential reproduces most properties of bulk water under ambient conditions. In particular, the model yields a correct static dielectric constant, which makes it appropriate to study systems dominated by water-mediated electrostatic interactions. The interaction energy of a single ion of charge $q = \pm|e|$ solvated in N water molecules is

$$U_{iw}(\{\boldsymbol{r}\}) = \frac{1}{2}k_D|\boldsymbol{r} - \boldsymbol{r}_D|^2 + \sum_{i=1}^{N}\sum_{s}\left[\frac{(q-\delta q)q_s}{|\boldsymbol{r} - \boldsymbol{r}_{is}|} + \frac{\delta q\, q_s}{|\boldsymbol{r}_D - \boldsymbol{r}_{is}|}\right] + \sum_{i=1}^{N} 4\epsilon_{IO}\left[\left(\frac{\sigma_{IO}}{|\boldsymbol{r} - \boldsymbol{r}_{iO}|}\right)^{12} - \left(\frac{\sigma_{IO}}{|\boldsymbol{r} - \boldsymbol{r}_{iO}|}\right)^{6}\right] \quad (1)$$

The vectors $\boldsymbol{r}$ and $\boldsymbol{r}_D$ are the positions of the ionic core and the ionic Drude particle, respectively. The ionic core has a charge $q - \delta q$ and the Drude particle has a positive charge δq (the sign of δq has no major consequences on the properties of the model[30]). The spring constant k_D is set to 1000 kcal/mol/Å^2. This value dictates the magnitude of the charge the Drude particle should carry to produce an ionic polarizability α:[28] $\delta q = \sqrt{\alpha k_D}$. In eq 1, the vector $\boldsymbol{r}_{is}$ is the position of site s of water molecule i. The SWM4-DP water model has five sites: the oxygen atom "O", the hydrogen atoms "H_1" and "H_2", a nonatomic site "M", and a Drude particle "D" (attached to the oxygen atom). Each of these sites has a charge q_s (see ref 21 for the values). The SWM4-DP model has a polarizability of 1.04252 Å^3 and uses $k_D = 1000$ kcal/mol/Å^2 as well, so $q_D = 1.77185|e|$. The ionic core is participating in Lennard-Jones (LJ) interactions with the oxygen atoms. The LJ parameters are combined according to the Lorentz−Berthelot rule,[31] $\epsilon_{IO} = \sqrt{\epsilon_I\epsilon_O}$ and $\sigma_{IO} = {}^1/_2\,(\sigma_I + \sigma_O)$. See ref 21 for the details on the water model.

2.2. Free Energy Calculations. The total solvation free energy ΔG_{tot} of a cation (anion), is calculated in three steps, as the total reversible thermodynamic work needed to first insert a neutral and nonpolarizable argon-like particle into the bulk phase, then transform this particle into a charged and polarizable potassium-like ion (or chloride-like ion in the case of an anion), and finally transform it into the final ionic species, yielding ΔG_1, ΔG_2, and ΔG_3, respectively. For the free energy calculations, the total potential energy of intermediate systems is defined as $U_{tot} = U_{ww} + \lambda U_{iw}$, where U_{ww} is the water−water potential energy, U_{iw} is the ion−water potential energy, and λ is a thermodynamic coupling parameter varying from 0 to 1. It should be noted that, because of the self-consistent field (SCF) induced polarization on all the dipoles in the system, the total potential energy U_{tot} is not truly pairwise decomposable. For instance, the induced dipoles $\{\boldsymbol{\mu}(\lambda)\}$ depend implicitly on the parameter λ, which couples the ion to the solvent. It follows that perturbations involving a charging process must be handled carefully to satisfy the SCF condition for all states. The most efficient approach to compute the free energy is to use thermodynamic integration (TI):

$$\begin{aligned}\Delta G_2 &= \int_0^1 d\lambda\, \frac{\partial}{\partial\lambda}\Delta G_2(\lambda) \\ &= \int_0^1 d\lambda \left[\left\langle \sum_i \frac{\partial U_{tot}(\{\boldsymbol{\mu}(\lambda)\};\lambda)}{\partial \boldsymbol{\mu}_i} \cdot \frac{d\boldsymbol{\mu}_i(\lambda)}{d\lambda}\right\rangle_{(\lambda)} + \left\langle \frac{\partial U_{tot}(\{\boldsymbol{\mu}(\lambda)\};\lambda)}{\partial\lambda}\right\rangle_{(\lambda)}\right] \\ &= \int_0^1 d\lambda\, \langle U_{iw}(\lambda)\rangle_{(\lambda)} \end{aligned} \quad (2)$$

because $\partial U_{tot}/\partial\boldsymbol{\mu}_i = 0$ according to the SCF condition. The free energy $\Delta G_{tot} = \Delta G_1 + \Delta G_2 + \Delta G_3$ corresponds to the reversible thermodynamic work of one ion going from vacuum to an infinitely dilute bulk solution. To convert those results to the process of an ion going from an ideal gas phase at 1 atm to an idealized bulk solution at 1 M concentration, the entropic contribution associated with confining 1 mol of ions from a volume of 24.465 L to a volume of 1 L, $-k_BT\ln(1/24.465) = 1.9$ kcal/mol, must be added (see also Supporting Information).

The reference, argon-like particle uses the LJ parameters $\epsilon = 0.2339$ kcal/mol and $\sigma = 3.4009$ Å (with no induced polarization). The insertion free energy is obtained from a calculation of the potential of mean force (PMF) of the LJ particle going across a slab of 125 SWM4-DP water molecules. The PMF is constructed using umbrella sampling and unbiased using the WHAM procedure.[32] From three replicas of the PMF calculation, we get $\Delta G_{hydr}(Ar) = +2.8$ kcal/mol. For the TI calculations, the ion is placed in the middle of a droplet of 250 explicit SWM4-DP water molecules, contained by the reactive spherical solvent boundary potential (SSBP).[33] The SSBP is an approximation that aims at simulating the properties of an infinite bulk water system using a finite number of explicit water molecules in a spherical region centered around the solute.[33]

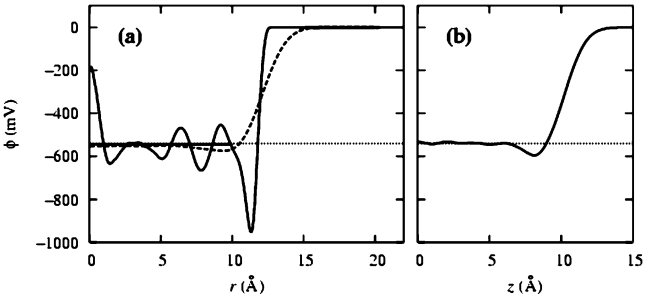

Figure 1. (a) Radial potential for 251 SWM4-DP molecules in SSBP, compared to (b) the potential profile across the water/air interface of a slab of 250 molecules.[21] In panel (a), the solid curve is the potential obtained from solving the radial Poisson equation $\nabla^2\phi(r) = -4\pi\rho(r)$, where $\rho(r)$ is the charge density obtained from a 1-ns simulation. The profile $\phi(r)$ displays spurious instabilities and oscillations for $r \rightarrow 0$ due to a lack of sampling in the vanishingly small volume, but this has no impact on the real average value. The solid horizontal line is a least-squares fit of $\phi(r)$ over the domain $0 < r < 10$ Å. For the fit, each point is given a weight proportional to $1/r^3$. The dashed curve is the radial potential obtained by assuming that the point charges have a Gaussian spatial spread of 1 Å. The dotted line indicates −540 mV, the air/water interface potential taken from panel (b).

Previous experience showed that it provides an accurate representation of the long-range electrostatic contribution with modest computational effort. Preliminary calculations with SSBP showed that 250 explicit water molecules is sufficient to avoid any significant finite-size effect on the estimated free energies. Nonetheless, the total free energy for solutes carrying a net charge must be interpreted correctly. In particular, the SSBP method produces a phase potential at the interface between the explicit water molecules and the surrounding continuum dielectric. As a net charge $\pm|e|$ is turned on in the middle of the explicit sphere of water, this interface potential contributes to the total free energy by a term $\pm F\phi_{\mathrm{SSBP}}$, where ϕ_{SSBP} is the potential created by the reorganization of the first few layers of water molecules inside the cavity in the SSBP continuum. This potential can be calculated by integrating the radial charge density obtained for a separate SSBP simulation without ions. This is shown in Figure 1. Remarkably, the interfacial potential in SSBP is nearly identical to the one from a simulation of a slab of explicit water in a vacuum. This observation holds for the SWM4-DP model used in this work (that is, $\phi_{\mathrm{SSBP}} \simeq -540$ mV) and also for the nonpolarizable TIP3P model.[34] One may note that there is a spurious numerical instability near the center of the sphere due to the vanishingly small volume element (varying like $4\pi r^2$), but this has no real impact on the average value affecting a finite solute; the fast oscillations of the potential near $r = 0$ are filtered if the point charges of the simulated system are replaced by Gaussians with a spread of 1 Å (see Figure 1). For a SSBP simulation performed with the TIP3P model, $\phi_{\mathrm{SSBP}} \simeq -500$ mV, the air/water potential for TIP3P.[35] Therefore, the charging free energy computed with SSBP effectively includes the interfacial potential contribution that an ion gains by crossing the physical interface from the gas phase to the bulk water. It follows that the results from those SSBP computations can readily be interpreted as "real" hydration free energies.

The free energy integral in eq 2 is computed as a discrete sum over 11 windows with $\lambda = 0, 0.1, 0.2, ..., 1$. To decrease possible hysteresis errors, the transformation is conducted "forward" and "backward", and the sampling is averaged. Each window is simulated with 10 ps of molecular dynamics, of which only the last 9 ps are used for the averaging. The 22 simulations are performed sequentially, going from $\lambda = 0$ to 1 and back to 0. The final configuration of each window serves as the initial configuration for the next. The first window uses a configuration equilibrated for 20 ps. The λ parameter turns on the charges on both the nuclear site I and the Drude particle D, so that both the ionic charge and the ionic polarizability are gradually introduced as λ goes from 0 to 1. The λ parameter also controls the switching from the LJ parameters of the argon model to the LJ parameters of the ion. In all the computations, room temperature (298.15 K) is maintained using a Nosé−Hoover thermostat[36] on the atoms. During the SSBP simulations, the radius of the spherical cavity responds dynamically to reproduce the ambient pressure. The Drude oscillators are maintained in the self-consistent field induction regime by being coupled to a second Nosé−Hoover thermostat at low temperature (1 K). See ref 28 for details on the simulation procedure. The equations of motion are integrated with a time step of 1 fs. All simulations are performed with the program CHARMM,[37] using the VV2 molecular dynamics module.[28] To extract the sensitivity of ΔG to the LJ parameters of the ions requires computations for a few hundred models. For that purpose, a simulation time of 10 ps per window is sufficient. For the final ion models, well-converged final values for the free energies were obtained using additional simulations with 100 ps per window (90 ps for averaging) and 200 ps for initial equilibration.

2.3. Characterization of Solvent Structure and Dynamics. To calculate the solvent structure, a single ion of each species is simulated in a cubic box of 500 SWM4-DP molecules with periodic boundary conditions (PBCs). The electrostatic interaction energy is summed up using the particle-mesh Ewald (PME) method.[38] The zero-wavevector contribution is not included in the fast Fourier transform in the PME calculations, so the total charge of the system ($+|e|$ or $-|e|$) is neutralized by a uniform charge background. Constant temperature (298.15 K) and pressure (1 atm) are maintained by coupling the atoms to a Nosé−Hoover thermostat[36] and a modified Andersen−Hoover barostat,[39] implemented in the VV2 module[28] of CHARMM.[37] The dynamics of the Drude oscillators is integrated as described previously. Five replicas of each simulation are equilibrated for 100 ps and average values are compiled for an additional 1000 ps, for a total of 5 ns of data for each ion type. The trajectories are saved every 0.1 ps and analyzed in segments of 100 ps. Radial distribution functions (RDFs) and average coordination numbers, $N(r) = \int \mathrm{d}r'\, 4\pi r'^2 g_{\mathrm{IO}}(r')$, are extracted from the PBCs simulations.

3. Target Data and Parametrization Strategy

3.1. Ionic Charges and Polarizabilities. In the current model, it is assumed that no charge transfer between the ions and the water molecules can take place. Several studies indicate that this a reasonable approximation, at least for monovalent cations and anions. Rashin et al.[40] have analyzed the electron density from DFT calculations of small hydrated ions (lithium, sodium, fluoride, and chloride) and shown that in ion−water clusters, spherical volumes containing full ionic charge of $\pm e$ have radii similar to the classical ionic radii.[40] This is indicative that charge redistribution for these monovalent ions can be accounted for by electronic polarization. In the model, particles are assigned a uniquely defined polarizability, which they carry both in the gas and in the condensed phase. This is certainly an approximation. From the analysis of the dispersion properties of alkali halide crystals,[41−44] it was found that the polarizability of atoms may be strongly affected by the dense packing of the crystalline environment. The smaller polarizability in the condensed phase may be rationalized with the following argument. In the gas

TABLE 1: Halide Ions Atomic Polarizabilities from the Literature (in Å^3) and the Values Used for This Work

	gas phase				liquid phase		
	ref 41[a]	ref 48[b]	ref 44[c]	ref 49[d]	ref 47[e]	ref 48[f]	current model[g]
F^-	1.38	2.24	2.495	2.467	1.20	1.30	1.786
Cl^-	3.94	5.65	5.545	5.482	3.65	3.76	3.969
Br^-	5.22	6.35	6.182	7.268	4.96	5.07	5.262
I^-	7.81	−	−	10.275	7.30	7.41	7.439

[a] Empirical estimation from refraction measurements of crystals. [b] Compilation of ab initio calculations from refs 57−59. [c] Ab initio calculations. [d] Ab initio calculations with relativistic corrections for Br^- and I^-. [e] Empirical estimation based on the compression effect of the solvent. [f] Empirical estimation. [g] This work (72.4% of ref 49).

phase, the polarizability of an atom in its ground state $|0\rangle$ may be expressed as a sum over excited states $|n\rangle$:

$$\alpha_{gas} = \sum_{n>0} \frac{\langle 0|\hat{\boldsymbol{\mu}}|n\rangle\langle n|\hat{\boldsymbol{\mu}}|0\rangle}{\epsilon_0 - \epsilon_n} \quad (3)$$

However, in the condensed phase, all extended electronic states with n greater than some excitation level n_e would overlap with the surrounding molecules and would, therefore, be forbidden by Pauli's exclusion principle. The resulting polarizability, which corresponds to the truncated sum

$$\alpha = \sum_{0<n\le n_e} \frac{\langle 0|\hat{\boldsymbol{\mu}}|n\rangle\langle n|\hat{\boldsymbol{\mu}}|0\rangle}{\epsilon_0 - \epsilon_n} \quad (4)$$

is thus expected to be smaller than the bare gas-phase value. This qualitative argument is supported by ab initio studies.[45,46]

Even though all studies do not agree on the importance of polarizability renormalization, they show that the effect is larger for halide ions and that it depends on the size and coordination of the counterions. A truly transferable model should account for this environment-dependent variation. For the sake of simplicity, we assigned a constant polarizability value to each anion in the halide series using a simple scheme. We use the "best" available estimates of the vacuum ionic polarizabilities and scale them down by a factor 0.724. All the results are summarized in Table 1. The renormalization effect is thought to decrease as the size of the ion increases.[47] Nonetheless, a constant renormalization factor is chosen here for the sake of simplicity. The resulting values are similar to those derived by Pyper et al.[48] The 0.724 factor corresponds to the renormalization for the molecular polarizability of the SWM4-DP water model.[21] SWM4-DP has $\alpha = 1.04252$ Å^3, which is 72.4% of 1.44 Å^3, the experimental value for a single water molecule in the gas phase. The "best" polarizabilities for the halide ions are taken from the time-dependent MP2 ab initio calculations of Hättig and Hess,[49] which include relativistic effects for the larger Br^- and I^- ions (see Table 1). Similar ab initio results are obtained by Jemmer et al.[44] (see Table 1). For chloride, 72.4% of 5.482 Å^3 is 3.969 Å^3. This is remarkably close to the solvent-renormalized value of 4 Å^3 inferred from Car−Parrinello simulations by Jungwirth and Tobias.[45] For fluoride, bromide, and iodide, the renormalized values are 1.786, 5.262, and 7.439 Å^3, respectively. The renormalized polarizabilities are somewhat larger than what many authors previously used for molecular dynamics simulations. More common values are around 1 Å^3 for fluoride,[50−52] between 4.5 and 4.8 Å^3 for bromide[52−54] (but sometimes as high as 5.5−5.8 Å^3; see ref 55), and between 5.3 and 6.9 Å^3 for iodide.[52−54,56] For fluoride, it could be argued that the polarizability should be smaller than 1.786 Å, because a smaller ion is more closely coordinated by the solvent, and its effective volume is smaller. However, a recent ab initio study[46] predicts a solvent-renormalized value somewhat closer to 1.786 Å^3 than to 1 Å^3 (between 1.346 and 1.636 Å^3 for fully hydrated states, compared to 2.405 Å^3 in the gas phase).

Unlike those of the halide ions, the polarizabilities of the alkali ions are not expected to be significantly changed by their coordination environment.[41] Accordingly, we use the gas-phase values reported by Mahan:[60] 0.032 Å^3 for Li^+, 0.157 Å^3 for Na^+, 0.830 Å^3 for K^+, 1.370 Å^3 for Rb^+, and 2.360 Å^3 for Cs^+. The exact α values are somewhat irrelevant for an empirical force field, because the induced polarizabilities are too small to affect the spherical symmetry of the solvent. Classical MD simulations of polarizable Na^+ in polarizable water[61] have shown that the electrostatic on the cation is not affected by any reasonable choice for the value of α.

TABLE 2: "Target" Binding Energies and Ion−Oxygen Distances for the Ionic Monohydrates

	U_{target}[a] (kcal/mol)	d_{ref}[b] (Å)		U_{target}[a] (kcal/mol)	d_{ref}[b] (Å)
Li^+	−34.0	1.87	F^-	−25.9	2.44
Na^+	−24.0	2.26	Cl^-	−14.4	3.11
K^+	−17.9	2.64	Br^-	−12.7	3.26
Rb^+	−15.9	2.79	I^-	−10.6	3.50
Cs^+	−13.7	2.99			

[a] Experimental binding enthalpies of Džidić and Kebarle[62] for alkali ions; ab initio results of Kim et al.[73] for halide ions. [b] Ion−oxygen distances calculated from ab initio geometries for K^+ and Cl^- (see text).

3.2. Ionic Monohydrates. The properties of ionic monohydrates are a fundamental piece of information in developing an optimal model. For the alkali ions, the target energy values are the binding enthalpies from the accurate gas-phase measurements of Džidić and Kebarle[62] (see Table 2). These values are in agreement with other experimental results[63,64] and with ab initio calculations.[65−72] For the halide ions, the target values are the ab initio binding energies of Kim et al.[73] (see Table 2). These energies agree with the very accurate results of Xantheas and Dang for fluoride[51] and chloride.[74]

The target reference ion−oxygen distances for the monohydrates can be extracted from ab initio calculations, though the results appear to be less reliable for the largest ions, such as rubidium, cesium, bromide, and iodide. For the sake of simplicity, the target reference distances for the ions larger than K^+ and Cl^- were estimated by using the corresponding difference in the ionic radii (R). For the alkali series, the ionic radii are:[75] 0.73 Å for Li^+ in a 4-coordinated crystalline environment, 1.16 Å for a 6-coordinated Na^+, 1.60 Å for a 7-coordinated K^+, 1.75 Å for an 8-coordinated Rb^+, and 1.95 Å for a 10-coordinated Cs^+. (It will be shown later that these coordination numbers are the integers closest to the actual coordination numbers obtained from the simulations.) For the halide series, the ionic radii are:[75] 1.19 Å for F^-, 1.67 Å for Cl^-, 1.82 Å for Br^-, and 2.06 Å for I^- (for 6-coordinated ions). The reference ion−oxygen distances for potassium and chloride ions are based on ab initio geometry optimizations of the monohydrates: 2.64 Å for potassium[66] and 3.11 Å for chloride.[73] For example, we use 2.64 Å − $R(K^+)$ + $R(Cs^+)$ for cesium and 3.11 Å − $R(Cl^-)$ + $R(I^-)$ for iodide. (See Table 2 for the complete series.) Such estimates are in close agreement with ab initio distances geometry optimization for the ions smaller than K^+ and Cl^-: 1.87 and 2.26 Å for lithium and sodium, respectively,[66] and 2.44 Å for fluoride.[73]

3.3. Absolute Free Energies of Hydration. Figure 2 summarizes some representative results taken from the literature (all converted to the same ideal standard states of 1 M in the

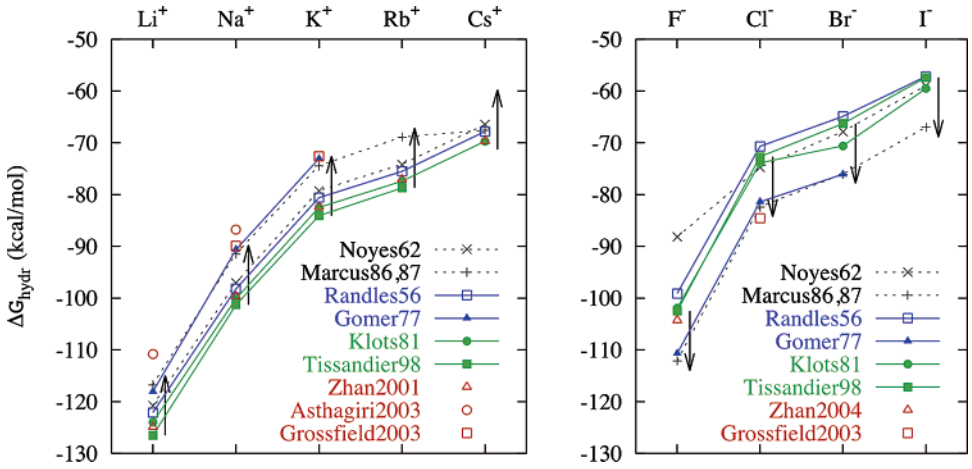

Figure 2. Survey of the intrinsic hydration free energies ΔG_{hydr}^{intr} for the alkali metal and halide ions. Noyes (ref 10) and Marcus (refs 11−13) are based on "classical" extrathermodynamic hypotheses, Randles (ref 9) and Gomer (ref 14) are based on eletrochemical measurements, Klots (ref 15) and Tissandier (ref 16) are based on extrapolation of gas-phase cluster measurements, and Zhan (ref 76), Asthagiri (ref 20), Grossfield (ref 6), and Zhan (ref 77) are theoretical predictions. All results have been converted to the following standard states: an ideal gas of ions at a pressure of 1 atm (where 1 mol of ions occupies a volume of 24.465 L), and an idealized 1 M ionic solution (with no ion−ion interactions).

TABLE 3: Values of the Air/Water Interface Potential Predicted by Various Water Models

model	ϕ (mV)	Fϕ (kcal/mol/e)
ST2[a]	−120	−2.77
TIP3P[b]	−500	−11.53
TIP4P[c]	−630	−14.53
SPC/E[d]	−550	−12.68
TIP4P−FQ[e]	−820	−18.91
RPOL[f]	−500	−11.53
SWM4-DP[g]	−540	−12.45

[a] Reference 78 (see ref 79 for the model). [b] Reference 35 (see ref 34 for the model). [c] Reference 78 (see ref 34 for the model). [d] Reference 80 (see ref 81 for the model). [e] Edward Harder, personal communication (see ref 82 for the model). [f] Reference 83 (see ref 84 for the model). [g] Reference 21.

solution and 1 atm in the gas phase).[6,9,10,12−16,20,76] For the sake of completeness, all the experimental and computational values are also provided in Supporting Information. Obviously, there is a significant spread among the different estimates of the hydration free energy of alkali halides. This poses a fundamental problem when trying to choose the appropriate experimental target data for the optimization of an accurate potential function. However, acknowledging the existence of a phase potential ϕ can possibly reconcile the spread in various estimates of the measured free energies. Values of the interfacial potential ϕ predicted by various water models are given in Table 3. Although there are some variations, the general trend appears to be quite robust: ϕ is negative and on the order of 0.5 V. The SWM4-DP water model used in this work yields an air/water interface potential of −540 mV.[21] The arrows in Figure 2 are illustrating the correction to the free energy for an air/water interface potential of −540 mV, that is, +12.45 kcal/mol for the monovalent cations and −12.45 kcal/mol for the monovalent anions. Most estimates fall well within the interval defined by the interfacial potential. This suggests that the differences between the various estimates of the hydration free energies may find their origin in whether the phase potential is, or not, incorporated. This observation has important implications on the parametrization strategy that we adopted to reproduce the target data on hydration free energies.

3.4. Parametrization Strategy and Sensitivity Analysis. Once the atomic polarizabilities of the ion models have been set, only the LJ parameters ϵ_I and σ_I remain to be determined. The Lennard-Jones potential obviously has a limited flexibility, and it is important to try to accommodate both the monohydrate properties as well as the bulk phase properties. To this end, we explore the range of solvation properties accessible by systematically varying the LJ parameters. Models requiring unphysical values of ϵ_I, smaller than 0.001 kcal/mol or larger than 0.5 kcal/mol, were not considered. For each ion model, LJ parameters corresponding to given values of the interaction energy with a single SWM4-DP water molecule, U_{min}, and ion−oxygen distance d_{min} were generated. The values of U_{min} and d_{min} were chosen to span, in increments of 0.25 kcal/mol for the energy and of 0.025 Å for the distance, the neighborhood of the best estimates of the ionic monohydrate (used as a target). For each LJ model corresponding to a pair $\{d_{min},U_{min}\}$, the real hydration free energy, ΔG_{hydr}^{real}, was computed using molecular dynamics simulations with explicit water molecules (following the method described above). The statistical errors on the individual estimations of ΔG were filtered out by the least-squares fit of a quadratic response-surface model (using six coefficients, a_0 to a_5)

$$\overline{\Delta G}(d_{min},U_{min}) = a_0 + a_1 d_{min} + a_2 U_{min} + a_3 d_{min}^2 + a_4 d_{min} U_{min} + a_5 U_{min}^2 \quad (5)$$

The polynomial is used to predict the free energy of interpolating ionic models. As long as the model has properties $\{d_{min},U_{min}\}$ within the region spanned by the original grid, the polynomial interpolation is more accurate than a single TI calculation. Figure 3 summarizes all the results concerning the response surfaces $\overline{\Delta G}$ in the $d_{min} - \Delta G_{hydr}$ plane. Each colored dot represents a tentative LJ model, for which the hydration free energy was computed (and used in the polynomial fit). The dots are laying on a band whose diagonal shape is due to the upper and lower limits imposed on the ϵ_I parameter. The color of each dot indicates the deviation of the monohydrate interaction energy (U_{min}) from the "target" value (U_{target}). For example, the orange dots are models within 0.25 kcal/mol of the target value, and the red dots are models where $U_{min} - U_{target} = -1.00$, −0.75, or −0.50 kcal/mol. The loci $U_{min} = U_{target}$ are traced with a black line (going through the orange region). The horizontal and vertical blue bars indicate the range of reasonable hydration free energies and ion−oxygen distances in the monohydrate. The thick horizontal lines are set to the "consensus" free energies of Tissandier et al.[16] (see Figure 2). The

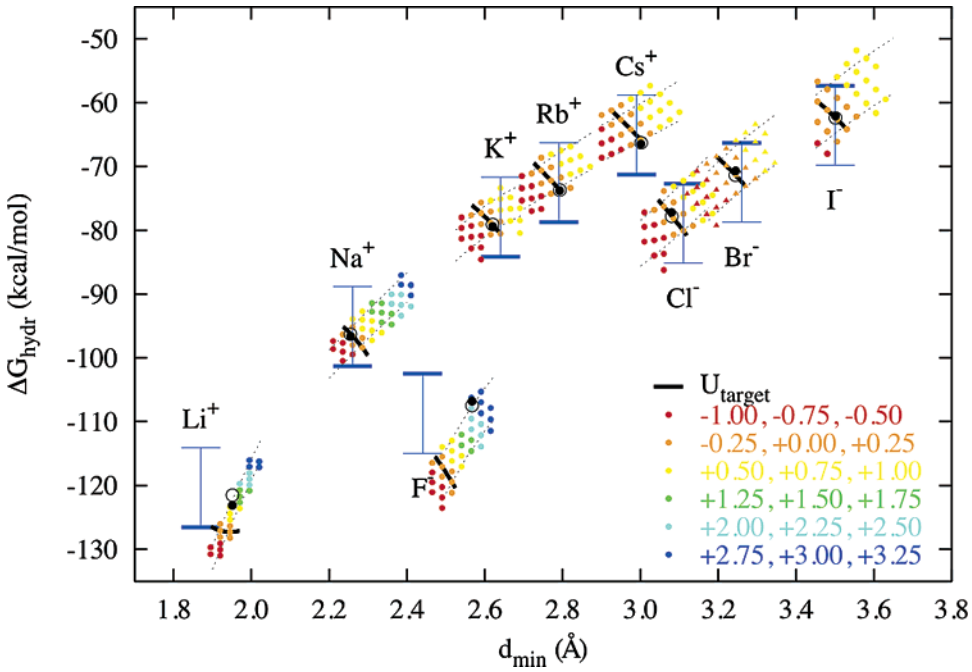

Figure 3. Mappings of the total hydration free energies in terms of the properties of the minimum-energy monohydrates (ion−oxygen distance, d_{min}, as *x*-coordinate, and interaction energy, U_{min}, color coded). The black circles and black dots correspond to the free energies of the AH/SWM4-DP model according to the polynomial prediction and according to the well-converged simulation results, respectively. Each colored dot represents a simulation realized for the LJ parameters of the ion reproducing a given pair of U_{min} and d_{min} values. The thick black lines are the loci where $U_{min} = U_{target}$ (see text for the values of U_{target}). The color code indicates different deviations from U_{target}, as listed on the legend (in kcal/mol). Orange indicates the smallest deviation: ±0.25 kcal/mol. The thick blue horizontal bars are the results of Tissandier et al.,[16] interpreted as ΔG^{real}_{hydr}, and the thin blue horizontal bars are the free energies corrected for the SWM4-DP phase potential. The blue vertical bars indicate the preferred geometries (see text and Table 2). For each species, oblique dotted curves show loci where $\epsilon_I = 0.01$ kcal/mol (top) and $\epsilon_I = 0.3$ kcal/mol (bottom).

thinner lines are 12.45 kcal/mol higher for the cations and 12.45 kcal/mol lower for the anions. If the energies marked by the thick lines were exactly equal to ΔG^{real}_{hydr}, then the thin lines would correspond to ΔG^{intr}_{hydr}.

Graphically, the ideal models should lie as close as possible to the intersection of the black line and the vertical blue line (i.e., have correct U_{min} and d_{min} for the monohydrates) and fall between the two horizontal blue lines (i.e., have correct hydration free energies). Simultaneously, the sum of the free energies of an ion and a counterion, $\Delta G^{intr}_{hydr}(M^+) + \Delta G^{intr}_{hydr}(X^-)$, and the difference of the free energies of two ionic species of the same sign, $\Delta G^{intr}_{hydr}(M_1^+) - \Delta G^{intr}_{hydr}(M_2^+)$, for the ideal models should match the experimental values as closely as possible.

The converged free energies (Table 5 and black dots on Figure 3) do not correspond exactly to the values predicted from the polynomial fit of eq 5 (black circles on Figure 3). Apart from the accumulation of statistical errors at every step of the free energy calculation, there is a small but significant error for $\Delta G(K^+ \rightarrow Li^+)$, which is 1.3 kcal/mol lower than predicted (see Table 5). This reflects the fact that some steps of the transformation into the highly structured hydration shell of Li^+ take slightly longer than 1 ps to equilibrate. A similar lack of equilibration may also explain the small +0.6 kcal/mol difference between the short and the long TI calculations of the Ar $\rightarrow Cl^-$ mutation. This error creates a small systematic deviation from the predictions of the free energies of the whole halogen series (see Figure 3).

4. Results and Discussion

A fundamental observation drawn from the systematic exploration of the parameters of the model shown in Figure 3 is that a unique absolute scale emerges naturally when one tries to accurately reproduce both the properties of monohydrates and the real hydration free energy, ΔG^{real}_{hydr}. Shifting this absolute scale of hydration free energy by a few kcal/mol toward more negative values would require using unphysically large values of the well-depth parameter ϵ. Alternatively, shifting the scale toward less negative values by a few kcal/mol becomes rapidly impossible because even vanishingly small values of ϵ do not alter the resulting hydration free energy. Recognizing that no absolute scale can be determined with certainty from the thermodynamic data, we use the constraints from the monohydrate geometries and binding energies to determine a consistent target reference for the real hydration free energy, ΔG^{real}_{hydr}. With the exception of lithium and fluoride, the smallest ions of each series, this scale is the only possibility in the context of the current model that allows the target monohydrate geometries and binding energies to be accurately reproduced while keeping the computed hydration free energies consistent with the thermodynamical data. This set of consistent free energies can be translated into a scale in which the intrinsic hydration free energy of the proton is −247 kcal/mol (assuming equilibrium between an ideal gas at 1 atm and an ideal solution of 1 M as reference states). In comparison, Tissandier et al.[16] find $\Delta G_{hydr}(H^+) = -264$ kcal/mol which, if one interprets their measurement as ΔG^{real}_{hydr}, would suggest $\Delta G^{intr}_{hydr}(H^+) \simeq -252$ kcal/mol. From their polarizable force field, Grossfield et al.[6] predict $\Delta G^{intr}_{hydr}(H^+) = -252.5$ kcal/mol.

The final set of parameters is presented in Table 4. It will be referred to as the AH/SWM4-DP model (AH standing for "alkali and halide"). In Table 4, the charges and polarizabilities for the model ions are compared with the gas-phase values of Mahan[60] and Hättig and Hess.[49] The properties of the ions in association with the SWM4-DP model are presented in Table 5. In Figure 3, the final models are indicated by black dots.

TABLE 4: Parameters of the Polarizable Ions

	q ($\|e\|$)	α^a (Å^3)	δq ($\|e\|$)	ϵ_I (kcal/mol)	σ_I (Å)
Li^+	+1	0.032 (0.032)	0.310427	0.00300	2.441062
Na^+	+1	0.157 (0.157)	0.687597	0.03151	2.583606
K^+	+1	0.830 (0.830)	1.580968	0.18290	2.931056
Rb^+	+1	1.370 (1.370)	2.031161	0.35190	3.118145
Cs^+	+1	2.360 (2.360)	2.665877	0.35760	3.527958
F^-	−1	1.786 (2.467)	2.319199	0.01000	4.026861
Cl^-	−1	3.969 (5.482)	3.457187	0.07658	4.383221
Br^-	−1	5.262 (7.268)	3.980713	0.10820	4.579218
I^-	−1	7.439 (10.275)	4.733085	0.15910	4.917760

[a] In parentheses are the ab initio estimates of the gas-phase polarizabilities (α_{gas}) from which the value are derived (see ref 60 for the alkali ions and ref 49 for the halide ions): $\alpha \equiv \alpha_{gas}$ for the alkali ions and $\alpha \equiv 0.724 \times \alpha_{gas}$ for the halide ions.

TABLE 5: Binding Energies and Ion−Oxygen Distances for the Minimum-Energy Monohydrates and "Real" Hydration Free Energies

	U_{min} (kcal/mol)	d_{min} (Å)	ΔG^{real}_{hydr} (kcal/mol)	$\Delta G^{intr\ a}_{hydr}$ (kcal/mol)	$\Delta\Delta G_{hydr}{}^b$ (kcal/mol)
Li^+	−32.538	1.951	−123.1	−110.6	−26.5 (−25.2)
Na^+	−24.000	2.255	−96.6	−84.1	−17.2 (−17.2)
K^+	−17.900	2.620	−79.4	−66.9	−5.6 (−5.4)
Rb^+	−15.900	2.792	−73.8	−61.3	−7.3 (−7.4)
Cs^+	−13.700	3.001	−66.5	−54.0	
F^-	−23.317	2.567	−106.8	−119.3	−29.6 (−29.7)
Cl^-	−14.400	3.080	−77.2	−89.7	−6.5 (−6.4)
Br^-	−12.700	3.244	−70.7	−83.2	−8.6 (−8.9)
I^-	−10.600	3.501	−62.1	−74.6	

[a] The "intrinsic" free energies are obtained by offsetting the energies by ±12.45 kcal/mol, the contribution from a SWM4-DP air/water potential interface. [b] Hydration energy differences along the series. The experimental values are in parentheses (see Table 1 of ref 16 and references therein; for Cs^+, see ref 15).

TABLE 6: Comparison of Calculated and Experimental Hydration Free Energies for Neutral Ion Pairs[a]

	F^-	Cl^-	Br^-	I^-
Li^+	−229.9	−200.3	−193.8	−185.2
	(−229.0)	(−199.3)	(−192.9)	(−183.9)
Na^+	−203.4	−173.8	−167.3	−158.7
	(−203.8)	(−174.0)	(−167.6)	(−158.7)
K^+	−186.2	−156.6	−150.1	−141.5
	(−186.6)	(−156.8)	(−150.4)	(−141.5)
Rb^+	−180.6	−151.0	−144.5	−135.9
	(−181.2)	(−151.4)	(−145.0)	(−136.1)
Cs^+	−173.3	−143.7	−137.2	−128.6
	(−173.8)	(−144.0)	(−137.6)	(−128.7)

[a] Energies in kcal/mol. Experimental values in parentheses (see Table 1 of ref 16 and references therein; for Cs^+, see ref 15).

Although the values of the LJ parameters were obtained after empirical adjustments to yield both consistent hydration free energies and properties of the ionic monohydrates, the latter are reproduced slightly less accurately in the case of lithium and fluoride. The limitations of the simple polarizable model are more apparent for the smallest ions of the series. The parameters of lithium and fluoride ions were therefore established by fixing ϵ_I at a reasonable value (0.003 kcal/mol for Li^+ and 0.01 kcal/mol for F^-) and then adjusting σ_I to best reproduce the hydration free energy.

4.1. Hydration Free Energies. The model reproduces the relative free energies within a series (see $\Delta\Delta G_{hydr}$ column of Table 5) as well as the total free energies of neutral ion pairs (see Table 6), which are all well-defined, measurable quantities. The free energies for the alkali series of the AH/SWM4-DP model are approximately 5 kcal/mol less negative than those of Tissandier et al.[16] (see Figure 2). In comparison, Asthagiri et al.[20] have obtained intrinsic hydration free energies for a selection of small ions (H^+, Li^+, Na^+, and OH^-) using the quasi-chemical framework with a quantum-mechanical description of the ion and its first solvation shell embedded into a classical molecular dynamics simulation. For Li^+ and Na^+, their results are about 15 kcal/mol higher than those of Tissandier et al.[16] Zhan and Dixon[76] have computed a value for the intrinsic hydration free energy of the proton comparable to that of Tissandier et al. (1.6 kcal/mol higher; see Figure 2) using ab initio electronic structure calculations of a proton solvated by a small number of water molecules embedded in a reactive continuum. Using a polarizable force field parametrized from ab initio gas-phase properties, Grossfield et al.[6] have obtained an absolute scale in which the intrinsic hydration free energy of the proton is 11.5 kcal/mol less negative than that of Tissandier et al. (see Figure 2).

Grossfield et al.[6] argue that the discrepancy between their prediction of $\Delta G^{intr}_{hydr}(H^+)$ and that of Zhan and Dixon[76] could arise from an irreducible contribution from the potential at the ion/water interface. Indeed, Ashbaugh has shown[85] that, in the limit of a fictitious ion of arbitrarily large size, the water molecules of the first solvation shell are expected to form an inverted interface similar to the air/water interface. This argument is useful for understanding why the TATB extrathermodynamic hypothesis is not valid but is irrelevant for the solvation of small ions, because the rearrangement of the solvent at the surface of a small ion (like H^+) is an intrinsinc contribution to the hydration free energy. Figure 2 suggests that the discrepancy might have an different origin. The calculation of Zhan and Dixon might include the contribution from a continuum/water interface potential, because the continuum does not prevent the explicit water molecules from creating a dipolar density at the interface. In contrast, free energy calculations based on simulations using periodic boundary conditions—such as the calculations of Asthagiri et al. and Grossfield et al.— do not include the phase potential contribution, because there is rigorously no physical vacuum/liquid interface.[86]

One may note that the contribution from the phase potential explains the large differences between the original free energy calculations of Beglov and Roux,[33] which led to the initial parametrization of the CHARMM force field for sodium, potassium, and chloride, and those carried out by Grossfield et al.[6] with the same model using PBCs and PME. The difference corresponds almost exactly to the contribution from crossing the air/water interface of TIP3P water ($\phi = -500$ mV and $\pm F\phi = \mp 11.53$ kcal/mol; see Table 3). It also suggests that the cluster measurements of Klots[15] and of Tissandier et al.,[16] as well as the calculations of Zhan and Dixon,[76] contain a contribution from the phase potential. This was previously noted by Asthagiri et al.[20]

Tissandier et al.[16] have extrapolated conventional free energy measurements on small ionic hydrates (ΔG°_n, where n is the number of water molecules) to obtain hydration free energies of ions in bulk phase. They argue that the gas-phase analysis does not include the phase potential because the measured clusters are too small for a genuine air/water interface to develop, and that it provides the intrinsic free energies ΔG^{intr}_{hydr}. We do not consider this argument very compelling. Rather, we agree with Grossfield et al.[6] that relating the quantity $\Delta G^\circ_n(M^+) - \Delta G^\circ_n(X^-)$ to the intrinsic hydration free energy of the proton does constitute an extrathermodynamic hypothesis. It is likely that, even for very small values of n, the outermost layers of water are not organized as they would be in bulk solvent, and

are creating a contribution to the hydration free energy that depends on the charge of the ion: $zF\phi_n$ instead of the bulk limit $zF\phi$. It is not yet clear how this surface reorganization potential goes to zero as the number of water molecules solvating the ion decreases.[87,88]

Figure 2 suggests an interpretation of the measured and calculated free energies that differs from the interpretations given by some of the authors. For the alkali series, assuming that the contribution from the phase potential is indeed close to −12 kcal/mol, the low energies may be considered estimates of $\Delta G^{\text{real}}_{\text{hydr}}$, and the high energies may be considered estimates of $\Delta G^{\text{intr}}_{\text{hydr}}$.

Such a consensus would require a revision of the interpretation of the measurements of Tissandier et al.[16] and the calculations of Zhan and Dixon[76] ($\Delta G^{\text{real}}_{\text{hydr}}$ instead of $\Delta G^{\text{intr}}_{\text{hydr}}$), but would confirm the interpretations of Asthagiri et al.[20] and Grossfield et al.[6] The present results, based on a systematic search for consistency with the AH/SWM4-DP model, yield an absolute free energy scale that differs somewhat from the previous consensus. However, it will be seen that the model yields excellent agreement with the ab initio data on small alkali hydrates.

4.2. Properties of Small Ion Hydrates. The AH/SWM4-DP model is parametrized for correct hydration energetics at infinite dilution. However, because the present effort is equally concerned by energetics and structure, it is important to examine the validity of the model by comparing its results with accurate results for small ion hydrates. Indeed, the zero-temperature hydrates are very revealing of how the competition between ion−water and water−water interactions is resolved for the different ions.[89]

Minimum energy clusters were generated by optimizing the geometry of many thousands of conformations of n molecules randomly placed and oriented around the ion. Tables 7 and 8 present the binding energies for the AH/SWM4-DP model. Only the lowest-energy clusters are reported. They are identified following the "n_1+n_2(S)" notation, where n_1 is the number of water molecules in the first solvation shell, n_2 is the number of water molecules in the second solvation shell, and S is the point-group symmetry. The structures are shown in Figures 4 and 5.

4.2.1. Alkali Hydrates: $M^+\cdot(H_2O)_{n=1-6}$. The binding energies of the alkali monohydrates were adjusted empirically to match exactly the experimental binding enthalpies of Ďzidić and Kebarle.[62] In the case of lithium, for which this constraint was incompatible with a consistent hydration free energy, the monohydrate binding energy differs by about 1.5 kcal/mol from the experimental value. Overall, it appears that, with good binding energies for the monohydrates, the polarizable model is remarkably able to reproduce the consensus ab initio energies of the larger clusters within a few percents (see Table 7). Many important structural effects are also reproduced accurately.

Dihydrates and Trihydrates. The most stable dihydrate is the "linear" 2+0(D_{2d}) structure for lithium and sodium, but the "bent" 2+0(C_2/C_s) structure for rubidium and cesium, as predicted by ab initio calculations.[90,66,70,72] For potassium, the most stable structure is 2+0(C_2/C_s), but the 2+0(D_{2d}) structure is only 0.024 kcal/mol higher. Scanning the O−K−O angle shows that the energy surface is extremely flat (within 0.03 kcal/mol) from 180° to 120°.

Trihydrates optimal structures are 3+0(D_3) for lithium, sodium, and potassium, and 2+1(C_{2v}) for rubidium and cesium, in agreement with ab initio calculations.[66,70,72] For rubidium, the 3+0(D_3) structure is the second most stable. For cesium, the second most stable structure has a broken symmetry 3+0-

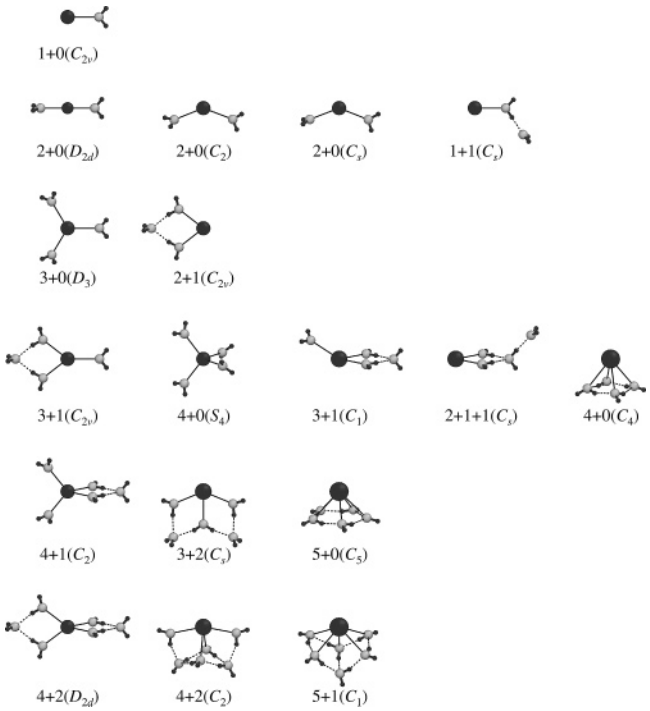

Figure 4. Illustration of the minimum-energy alkali−aqua clusters with their structure names. All structures are shown for potassium, except the 2+0(D_{2d}) structure (shown for sodium), the 3+1(C_1), 2+1+1(C_1), 3+2(C_s), and 4+2(C_2) structures (shown for rubidium), and the 4+0-(C_4), 5+0(C_5), and 5+1(C_1) structures (shown for cesium).

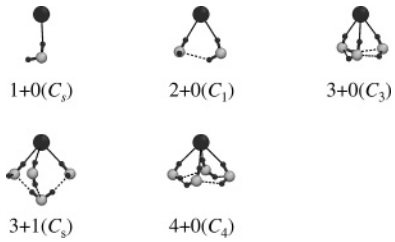

Figure 5. Illustration of the minimum-energy halide−aqua clusters with their structure names. All structures are shown for chloride.

(C_3), because the three water molecules can optimize their mutual interaction by having the ion out of the plane.

Tetrahydrates. The lowest-energy lithium tetrahydrate is the 4+0(S_4) structure, for which the four water molecules are in the first solvation shell. It is the most stable structure for sodium as well. For both lithium and sodium, the 3+1(C_{2v}) structure (with a water molecule in the second shell) has a higher energy. The ab initio calculations of Glendening and Feller[66] give the same ordering for lithium but the reverse for sodium—although not by a large energy difference. This reversal, along with the fact that the energy of the 3+0(D_3) sodium trihydrate structure is low compared to the ab initio estimates, could be an indication that the sodium−water interaction is slightly too favorable compared to the water−water interaction. For potassium, the 3+1(C_{2v}) structure is more stable than the 4+0(S_4) structure, in agreement with ab initio results.[66,70,72] For rubidium, the lowest-energy tetrahydrate is a 3+1(C_{2v}) structure "broken" into a 3+1(C_1) structure. The water molecule not involved in any water−water hydrogen bond is bent away from the mirror plane (see Figure 4). Energetically, this structure is comparable to the ab initio 3+1(C_2) structure of Glendening and Feller.[66] For cesium, the lowest-energy structure is 4+0(C_4), where the four water molecules form a cyclic tetramer on one side of the ion. The lowest-energy ab initio structure predicted by Glendening

TABLE 7. Lowest-Energy Alkali Hydrates for $n = 1-6$ Water Molecules[a]

			AH/SWM4-DP model		ab initio calculations					
	n	structure[b]	$-U$	d	$-U$	d	$-U$	d	$-U$	d
					Reference 66[c]		Reference 65[d]		Reference 69[e]	
Li^+	1	1+0(C_{2v})	**32.538**	1.951	**34.5**	1.850	**35.2**	1.847	**33.8**	1.849
	2	2+0(D_{2d})	**61.436**	1.968	**64.4**	1.878	**64.0**	1.884	**63.5**	1.875
		1+1(C_s)	**47.699**	1.927, 4.170	**51.1**	1.810, 3.977	**52.4**	1.835		
	3	3+0(D_3)	**84.346**	1.997	**87.5**	1.915	**86.8**	1.927	**86.5**	1.915
	4	4+0(S_4)	**101.780**	2.036	**104.1**	1.969	**104.3**	1.971	**103.2**	1.968
		3+1(C_{2v})	**98.092**	1.996, 3.694	**103.1**	1.911, 3.689	**103.3**	1.916, 1.928		
	5	4+1(C_2)	**114.943**	2.035, 3.768	**118.5**	1.966, 3.816	**119.3**	1.959, 1.970	**117.1**	1.966
	6	4+2(D_{2d})	**127.377**	2.037, 3.792					**130.3**	1.965
					Reference 66[c]		Reference 67[f]			
Na^+	1	1+0(C_{2v})	**24.000**	2.255	**24.3**	2.230	**23.7**	2.228		
	2	2+0(D_{2d})	**45.675**	2.273	**45.5**	2.249	**44.9**	2.253		
		1+1(C_s)	**37.651**	2.223, 4.395	**38.9**	2.185, 4.233				
	3	3+0(D_3)	**64.138**	2.295	**63.5**	2.277	**62.9**	2.282		
	4	4+0(S_4)	**79.522**	2.320	**77.5**	2.306	**77.5**	2.317		
		3+1(C_{2v})	**77.782**	2.293, 3.997	**78.0**	2.268, 4.027				
	5	4+1(C_2)	**92.597**	2.318, 4.044	**91.0**	2.300, 4.118	**90.7**	2.312, 4.149		
	6	4+2(D_{2d})	**105.298**	2.319, 4.064			**103.7**	2.307, 4.180		
					Reference 66[c]		Reference 70[g]		Reference 72[h]	
K^+	1	1+0(C_{2v})	**17.900**	2.620	**18.9**	2.669	**17.4**	2.639	**17.8**	
	2	2+0(C_2)	**33.988**	2.642						
		2+0(C_s)	**33.988**	2.643						
		2+0(D_{2d})	*__33.964__	2.644	**35.8**	2.707	**32.9**	2.673	**33.5**	
		1+1(C_s)	**30.276**	2.575, 4.667	**31.7**	2.603, 4.611	**30.1**	2.567, 4.424		
	3	3+0(D_3)	**48.440**	2.661	**50.9**	2.730	**46.9**	2.690	**47.1**	
		2+1(C_{2v})	**47.890**	2.624, 4.348	**49.8**	2.662, 4.433	**47.1**	2.625, 4.354	**48.8**	
	4	3+1(C_{2v})	**61.818**	2.658, 4.366	**64.1**	2.719, 4.474	**60.2**	2.681, 4.384	**62.2**	
		4+0(S_4)	**61.083**	2.681	**63.7**	2.759	**58.9**	2.713	**59.1**	
	5	4+1(C_2)	**73.976**	2.677, 4.398	**76.4**	2.747, 4.542	**71.6**	2.703, 4.438		
	6	4+2(D_{2d})	**86.616**	2.673, 4.411			**84.0**	2.693, 4.451	**85.6**	
					Reference 66[c]					
Rb^+	1	1+0(C_{2v})	**15.900**	2.792	**16.1**	2.902				
	2	2+0(C_2)	**30.238**	2.814	**30.7**	2.933				
		2+0(C_s)	**30.237**	2.813, 2.815	**30.7**	2.933, 2.934				
		1+1(C_s)	**27.785**	2.741, 4.795	**28.2**	2.832, 4.823				
	3	2+1(C_{2v})	**44.073**	2.791, 4.525	**44.2**	2.889, 4.672				
		3+0(D_3)	**43.212**	2.835	**43.7**	2.960				
	4	3+1(C_1)	**56.437**	2.829, 4.540	**56.6**	2.948, 4.699[i]				
		2+1+1(C_s)	**55.110**	2.780, 4.447, 6.613						
		4+0(S_4)	**54.802**	2.853	**55.1**	2.987				
	5	3+2(C_s)	**67.948**	2.791, 2.820, 4.576						
		4+1(C_2)	**67.569**	2.834, 2.859, 4.565						
	6	4+2(C_2)	**80.434**	2.812, 2.971, 3.874						
		4+2(D_{2d})	**80.078**	2.841, 4.575						
					Reference 66[c]					
Cs^+	1	1+0(C_{2v})	**13.700**	3.008	**14.1**	3.136				
	2	2+0(C_s)	**26.122**	3.027, 3.031	**26.8**	3.168, 3.171				
		2+0(C_2)	**26.121**	3.029	**26.8**	3.169				
		1+1(C_s)	**25.037**	2.948, 4.962	**25.5**	3.055, 5.033				
	3	2+1(C_{2v})	**39.771**	2.999, 4.745	**39.8**	3.117, 4.909				
		3+0(C_3)	**37.398**	3.050	**38.2**	3.201[i]				
	4	4+0(C_4)	**50.817**	3.163	**53.0**	3.323				
		2+1+1(C_s)	**50.607**	2.986, 4.663, 6.832						
		3+1(C_1)	**50.452**	3.040, 4.765	**50.6**	3.152, 3.223, 4.934[j]				
	5	5+0(C_5)	**63.174**	3.198						
	6	5+1(C_1)	**74.561**	3.140, 3.167, 3.167, 3.190, 3.210, 3.981						
		4+2(C_2)	**74.407**							

[a] *U* columns are binding energies (in kcal/mol) and *d* columns are ion−oxygen distances (in Å). Degenerate distances are listed only once. For comparable distances, only the average is given. * = Unstable conformation. [b] See Figure 4 for an illustration of the structures. [c] MP2/6-31+G*//RHF/6-31+G* level. [d] MP2/CBS level for $n = 1$, MP2/aug-cc-pVQZ//MP2/aug-cc-pVTZ level from $n = 1$ to 2 (but MP2/aug-cc-pVDZ level for the 1+1(C_s) structure), and MP2/aug-cc-pVDZ for $n = 2$ to 3, $n = 3$ to 4, and $n = 4$ to 5. [e] MP2/6-31++G(d,p)//HF/6-31++G(d,p) level with counterpoise correction. [f] MP2/TZ2P level with BSSE correction. [g] MP2/TZ2P level with BSSE correction. [h] MP2/aug-cc-pVTZ level. [i] 3+0(D_3) structure. [j] 3+1(C_2) structure.

and Feller is 4+0(C_4).[66] Somewhat surprisingly, the second most stable structure for both rubidium and cesium is the 2+1+1-(C_s) structure, with a molecule in the third shell (see Figure 4). This preference could be explained by the binding cooperativity in the SWM4-DP water model, enhanced by a significant polarization of the water molecules in the first and second shells. In the 2+1+1(C_s) hydrates, the water molecule involved in three hydrogen bonds is actually more polarized than the two in proximity of the ion. To our knowledge, this 2+1+1 structure has not been reported in previous ab initio studies.

TABLE 8: Lowest-Energy Halide Hydrates for $n = 1-4$ Water Molecules[a]

			AH/SWM4-DP model		ab initio calculations			
	n	structure[b]	$-U$	d	$-U$	d	$-U$	d
					Reference 73[c]			
F^-	1	1+0(C_s)	**23.317**	2.567	**25.9 ± 1.5**	2.436		
	2	2+0(C_1)	**45.596**	2.587, 2.579	–	–		
	3	3+0(C_3)	**67.264**	2.600	**63.7 ± 3.7**	2.582		
	4	4+0(C_4)	**83.907**	2.647	**78.3 ± 4.9**	2.670		
		3+1(C_s)	**83.688**	2.588, 2.619, 3.669				
					Reference 73[c]		Reference 74[d]	
Cl^-	1	1+0(C_s)	**14.400**	3.080	**14.4 ± 1.2**	3.108	**13.8**	3.136
	2	2+0(C_1)	**29.965**	3.111, 3.082	**28.6 ± 2.7**	3.177	**27.5**	3.105, 3.276
	3	3+0(C_3)	**46.950**	3.119	**42.9 ± 4.2**	3.211	**41.9**	3.223
	4	3+1(C_s)	**61.714**	3.056, 3.126, 4.096				
		4+0(C_4)	**61.457**	3.149	**56.2 ± 5.7**	3.272	**54.1**	3.270
					Reference 73[c]			
Br^-	1	1+0(C_s)	**12.700**	3.244	**12.7 ± 0.9**	3.316		
	2	2+0(C_1)	**27.076**	3.240, 3.286	**25.8 ± 2.1**	3.389		
	3	3+0(C_3)	**43.353**	3.288	**39.7 ± 3.6**	3.403		
	4	4+0(C_4)	**57.421**	3.316	**52.6 ± 5.0**	3.458		
		3+1(C_s)	**57.327**	3.203, 3.287, 4.248				
					Reference 73[c]		Reference 95[e]	
I^-	1	1+0(C_s)	**10.600**	3.501	**10.6 ± 0.6**	3.632	**10.43 ± 0.63**	3.59
	2	2+0(C_1)	**23.490**	3.483, 3.570	**22.3 ± 1.5**	3.718	**22.38 ± 1.49**	3.64
	3	3+0(C_3)	**38.863**	3.552	**35.4 ± 2.9**	3.700	**36.48 ± 2.37**	3.69
	4	4+0(C_4)	**52.309**	3.580	**48.0 ± 4.3**	3.743	**49.26 ± 3.66**	3.69
		3+1(C_s)	**51.466**	3.437, 3.548, 4.490			**47.09 ± 3.45**	3.62, 4.49

[a] *U* columns are binding energies (in kcal/mol) and *d* columns are ion−oxygen distances (in Å). Degenerate distances are listed only once. For comparable distances, only the average is given. [b] See Figure 5 for an illustration of the structures. [c] MP2/6-311++G** level. [d] MP2/aug-cc-pVDZ level with BSSE correction. [e] MP2/aug-cc-pVDZ+diff level. For the 2+0(C_1) and 3+1(C_1) structures, the ion−oxygen distances are averages.

Pentahydrates. The most stable pentahydrate structures are 4+1(C_2) for lithium, sodium, and potassium, 3+2(C_s) for rubidium, and 5+0(C_5) for cesium (see Figure 4). For rubidium, the 4+1(C_2) structure is only 0.379 kcal/mol above the deepest energy minimum. For cesium, it has an energy 3.015 kcal/mol above that of 5+0(C_5).

Hexahydrates. The symmetry of the lowest-energy hexahydrate structure appears to be very sensitive to the size of the ion. The approximately tetrahedral coordination of the 4+2(D_{2d}) structure accommodates better a small ion, while the looser, asymmetric coordination of the 4+2(C_2) structure is compensated by six water−water hydrogen bonds (instead of four for the D_{2d} structure). For lithium, the model predicts that the D_{2d} structure has the lowest energy; the C_2 conformer is not stable. For sodium, the energy of the 4+2(C_2) structure is 3.653 kcal/mol above the global minimum, in accord with the ab initio calculations of Feller.[91] Within this energy interval, the model predicts many other conformers, including one with a water molecule in the third solvation shell. For potassium, the model predicts that D_{2d} has the lowest energy, but the C_2 structure is second-lowest, 1.000 kcal/mol above. This is in contrast with the calculations of Lee et al.,[70] who predicted C_2 to be more stable than D_{2d} by a few kcal/mol. For rubidium, the two structures have comparable energies, C_2 being more stable by 0.355 kcal/mol. Cesium, which is big enough to allow water−water hydrogen bonding within its first solvation shell, is an exception. Its energy minimum is a 5+1(C_1, pseudo-C_s) structure formed by a "book" water hexamer distorted to accommodate its contact with the ion. The second-lowest-energy structure is 4+2(C_2), 0.154 kcal/mol above. The 4+2(D_{2d}) structure of cesium is 2.139 kcal/mol above the global minimum, higher than many other conformers with water−water hydrogen bonds within the first solvation shell.

4.2.2. Halide Hydrates: $X^-\cdot(H_2O)_{n=1-4}$. Because the halide ions are known to severely disrupt the tetrahedral arrangement of water, the minimum-energy halide hydrates represent a stringent test of the current model. The monohydrates have a C_s symmetry, with one hydrogen atom pointing toward the ion. For the dihydrates, it is known that the two water molecules form a distorted dimer on the same side of the ion—except for fluoride, which is strong enough to break the water dimer.[92] It may be that the water model, whose hydrogen sites were parametrized for normal hydrogen bonding, describes the close hydrogen−hydrogen contacts forced by a strong anion less accurately.

Table 8 presents the lowest-energy halide hydrates structures. The monohydrates are as in Table 5. Except for the monohydrate energies (that were target values), the binding energies are overestimated. The structures are illustrated in Figure 5.

For the fluoride dihydrate, the model produces an O−F−O angle of 73.2°, much narrower than the ab initio predictions of about 100°.[51,92] Ab initio calculations predict an open structure where the two water molecules are unbound, but the model produces a structure similar to those of chloride, bromide, and iodide dihydrates. In contrast, the model seems unable to stabilize a dihydrate structure with no water−water hydrogen bond. Figure 6a shows the energy profile of the model as the O−F−O angle is opened, compared to the same profile from an ab initio calculation at the MP2/6-311++G** level of theory (the same level used by Kim et al.[73] in their study of small halide hydrates) performed using Gaussian 98.[93] The ab initio energy surface shows that the minimum-energy angle is about 130° at the MP2/6-311++G** level (with rigid water molecules kept in the SWM4-DP geometry). The MP2/6-31G* level cannot reproduce the breaking of the intra-shell hydrogen bond, and it has a minimum at about the same angle as the model. This imbalance is noticeable for chloride as well (see Figure 6b), and although the model picks the correct minimum-energy conformation, its stability is overestimated compared to the MP2/6-311++G** level calculation. In contrast with ab initio predictions,[94] the "bound" state is probably too stable for the "open" state to become thermodynamically stable at room temperature. This suggests that the SWM4-DP model does not

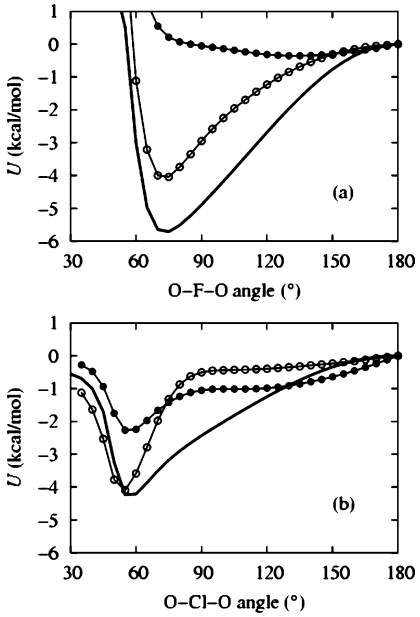

Figure 6. Binding energies for (a) fluoride dihydrate and (b) chloride dihydrate as a function of the O−Ion−O angle. Filled symbols are the MP2/6-311++G** calculations and the open symbols are MP2/6-31G* calculations. Solid lines are the results from the AH/SWM4-DP model. Ab initio calculations are done with the water molecules maintained in the SWM4-DP geometry (l_{OH} = 0.9572 Å and θ_{HOH} = 104.52°). The conformation with an O−Ion−O angle of 180° is the energy reference point.

provide enough repulsion when two adjacent water molecules are coordinating a very small anion.

The most stable halide trihydrates all have a 3+0(C_3) structure (see Figure 5). The second-lowest-energy structure (not shown in Figure 5) has one of the three water−water bonds broken, but is 2.1 kcal/mol above the 3+0(C_3) minimum energy for fluoride and even less stable for the larger halogen ions. With the exception of chloride, the optimal halide tetrahydrates are 4+0(C_4) structures, as predicted by ab initio calculations.[73] Along with this well-documented minimum-energy structure is a pyramidal 3+1(C_s) structure (see Figure 5). A pyramidal isomer was predicted for fluoride by Bryce et al.[96] (who used both ab initio calculations and a polarizable model) and shown consistent with vibrational spectroscopy measurements by Robertson et al.[97] Using an additive molecular mechanical model, Duan and Zhang[98] found the lowest-energy chloride tetrahydrate to be a pyramidal structure as well. What is unusual about the structure predicted by the current model is that the dangling hydrogen atoms of the two first-shell water molecules are pointing *toward* the oxygen of the third first-shell molecule. This, again, points to limitations in the hydrogen repulsive interactions in the SWM4-DP model.

The experimental pentahydrates and hexahydrates have the interesting property of allowing thermodynamically stable *internal* hydration states[99,100] (states for which the ion is solvated on all sides). Because of the understimation of the hydrogen−hydrogen short-range repulsion, the model does not indicate this transition to clusters with internal ions. Instead, the few most stable structures are "4+1" and "4+2" surface clusters with water molecules very densely packed on one side of the ion, all along the series from fluoride to iodide.

4.3. Solvation Structure in the Bulk Phase. Ion−oxygen and ion−hydrogen radial distribution functions (RDFs) $g_{IO}(r)$ and $g_{IH}(r)$ as well as the running coordination numbers $N(r)$ are extracted from the solvent box simulations (see Figures 7 and 8). The positions and amplitudes of the extrema are presented in Table 9 along the oxygen coordination numbers for the first shell, $N_c = N(r_{min1})$, and second shell, $N_{c2} = N(r_{min2}) - N(r_{min1})$.

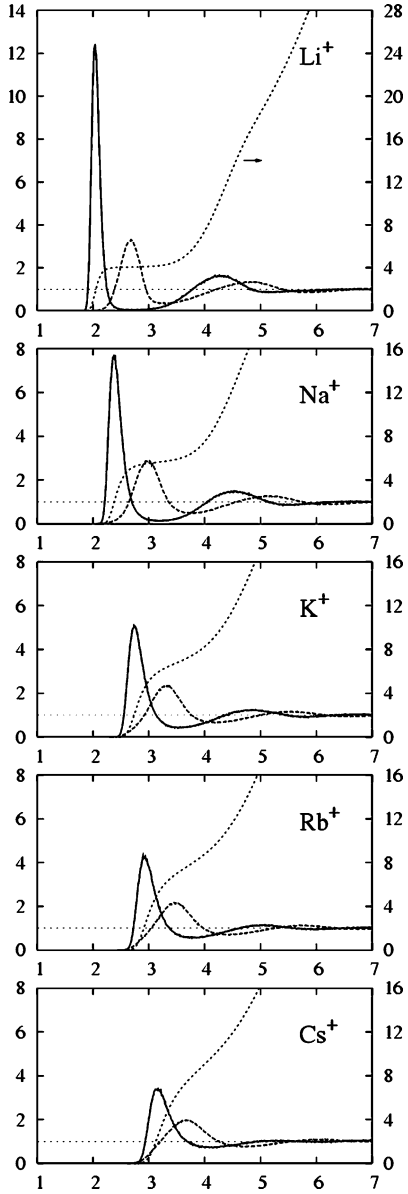

Figure 7. Radial hydration structure of the alkali ions for the AH/SWM4-DP model. The $g_{IO}(r)$ functions are solid lines, the $g_{IH}(r)$ functions are dashed lines (referring to the left axis), and the $N(r)$ functions are dotted lines (referring to the right axis) Distances are in Å.

4.3.1. Alkali Ions. In accordance with the most recent computational studies,[101−105] the current model predicts that the lithium ion is basically 4-coordinated (see Figure 7 and Table 9). (Table 1 of ref 104 provides a survey of the literature.) The first peak of $g_{LiO}(r)$ is at 2.03 Å, a distance comparable to recent results from quantum molecular dynamics (1.96 Å[102] and 1.93 Å[103]) and within the experimental range obtained from neutron and X-ray diffraction (1.94−2.07, see Table 1 of ref 104 and references therein). The $g_{LiO}(r)$ function has a deep first minimum (see Figure 7 and Table 9), in agreement with the Car−Parrinello (CP) simulations of Lyubartsev et al. (who get $g_{min1} = 0.015$),[102] but somewhat in disagreement with the QM/MM simulations of Loeffler and Rode,[103] who obtain a more populated inter-shell region. A strongly depopulated inter-shell region makes the exchange of water molecules between the first

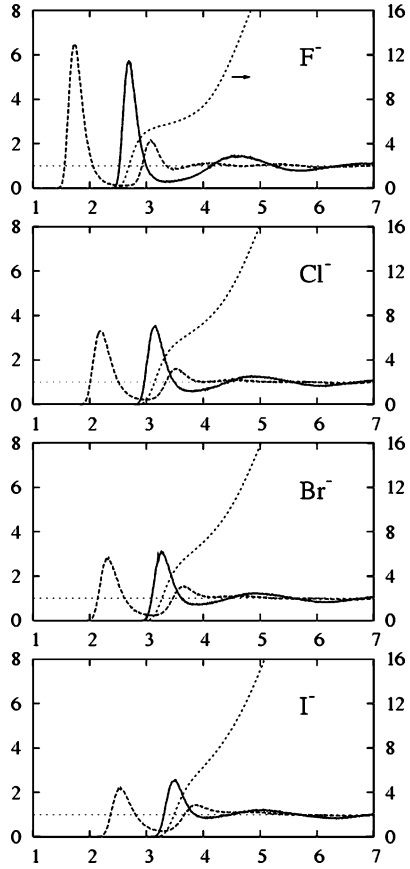

Figure 8. Radial hydration structure of the halide ions for the AH/SWM4-DP model. The $g_{IO}(r)$ functions are solid lines, the $g_{IH}(r)$ functions are dashed lines (referring to the left axis), and the $N(r)$ functions are dotted lines (referring to the right axis). Distances are in Å.

TABLE 9: Summary of the Radial Hydration Structures for the AH/SWM4-DP Model

	r_{max1} (Å)	g_{max1}	r_{min1} (Å)	g_{min1}	N_c	r_{max2} (Å)	g_{max2}	r_{min2} (Å)	g_{min2}	N_{c2}
Li^+	2.03	12.4	2.74	0.039	4.08	4.28	1.62	5.17	0.865	16.0
Na^+	2.37	7.65	3.21	0.141	5.67	4.53	1.47	5.50	0.868	18.3
K^+	2.74	5.05	3.55	0.431	6.90	4.84	1.23	5.80	0.915	20.2
Rb^+	2.92	4.23	3.80	0.576	8.00	5.04	1.13	5.94	0.955	20.7
Cs^+	3.15	3.40	4.10	0.728	9.55	5.25	1.03	6.05	0.982	20.2
F^-	2.69	5.69	3.36	0.287	5.74	4.61	1.43	5.69	0.784	20.0
Cl^-	3.14	3.51	3.79	0.592	6.50	4.88	1.25	6.07	0.831	23.3
Br^-	3.27	3.25	3.90	0.720	6.59	4.91	1.22	6.16	0.832	24.1
I^-	3.49	2.53	4.07	0.855	6.70	5.00	1.20	6.35	0.840	26.1

and second hydration shells less frequent. The current model for lithium has 16.0 molecules in the second hydration shell, in accord with recent classical MD simulations of a nonadditive force field (16 and 18 molecules, depending on the model)[105] but in contrast with QM/MM simulations (13 molecules)[103]—which may suffer from a finite-size effect.

For sodium, the current model predicts an average of 5.67 water molecules in the first solvation shell, in good agreement with the QM/MM simulations of Tongraar et al.[106] (5.6 ± 0.3), the ab initio MD simulations of White et al.[107] (5.2), and other classical polarizable MD simulations (5.7[3] and 5.56[108]) but in disagreement with the QM/MM simulations of Rempe and Pratt[109] (4.6). The AMOEBA polarizable force field of Grossfield et al.[6] gives $N_c = 6.0$. The position of the maximum at 2.37 Å is close to previous values from ab initio and classical nonadditive MD simulations (2.33,[106] 2.49,[107] and 2.37 Å[108]). The model has 18.3 molecules in the second solvation shell of sodium, compared to 16 for the ab initio MD of White et al.[107]

For potassium, the model predicts 6.90 water molecules in the first shell, in agreement with the ab initio CP simulation of Ramaniah et al. (6.75).[110] The AMOEBA model[6] predicts a comparable 7.0. In contrast, the recent polarizable model of Carrillo-Tripp et al.[108] produces a significantly higher coordination (7.85 ± 0.48). A similar coordination is obtained in a QM/MM simulation by Tongraar et al.[106] (8.3 ± 0.3). In the same work, Tongraar et al. obtain a coordination of 7.8 ± 0.2 from a pairwise-additive model parametrized against an ab initio energy surface.[106] X-ray[111] and neutron[112] scattering experiments suggest that the potassium ion is 6-coordinated, although a more sophisticated analysis[113] of the neutron data proposes a coordination of 7.5. The position of the first peak of the $g_{KO}(r)$ function is 2.74 Å, at a slightly shorter distance than the consensus experimental value proposed by Marcus[114] (2.80 Å), the CP simulations result of Ramaniah et al.[110] (2.81 Å), and the MD results of Carrillo-Tripp et al.[108] (2.79 Å). The first peak is slightly higher than the CP result of Ramaniah et al.: 5.05 compared to 3.44.[110]

For rubidium and cesium, the AH/SWM4-DP model yields $N_c = 8.00$ and 9.55, respectively. Recent QM/MM simulations indicate $N_c = 7.1$ for rubidium[115] and about 9 for cesium.[116] X-ray absorption[117−119] and neutron scattering[120] studies on rubidium suggest a 6-coordination with ion−oxygen distances of about 2.9 Å, and X-ray studies on hydrated cesium suggest an 8-coordination.[121]

Overall, the average structural results are acceptable given that no direct adjustment to the shape of the RDFs was made for any ion. The first hydration shell of sodium and lithium appears to be slightly more rigidly structured than suggested by other results. For lithium, the first peak of the $g_{LiO}(r)$ distribution is high (12.4) compared to the ab initio simulations of Lyubartsev et al. (∼9.5)[102] and of Loeffler and Rode (∼8.5).[103] MD simulations of nonadditive force fields give comparable low maxima (∼9.8[103] and ∼8.2[104]). For sodium, the first peak of the $g_{NaO}(r)$ distribution is higher and the first minimum is lower than the results from ab initio simulations[106,107] and X-ray results.[122] The model for sodium gives $g_{max1} = 7.65$ and $g_{min1} = 0.141$, while the experimental values are around 3.5 for g_{max1} and 0.5 for g_{min1}.[122,107] The enhanced structure, observed more prominently in the case of lithium and sodium, could be partly due to the "hardness" of the Lennard-Jones 6−12 potential. The steep 12th power repulsion does not allow large radial fluctuations for a molecule in the first shell of the ion, which leads to a sharp peak. The rigidity of the molecular geometry of the SWM4-DP model may also play a role, though it is unclear whether allowing flexibility would enhance or weaken the local structure.[123,124] However, one should also note that several estimates from diffraction experiments or CPMD simulations correspond to systems at much higher concentrations (≃3 M for diffraction experiments and 1 ion for ≃50 water molecules in CPMD), whereas the current results from the AH/SWM4-DP model correspond to very high dilution (1 ion per 500 water molecules). Decreasing the number of water molecules available per ion disrupts the first shell and leads to a smaller first peak in the radial distribution function. Generally, the current AH/SWMD4-DP model displays hydration structures and hydration free energies that are quite similar to those of the standard nonpolarizable model of Åqvist.[125] The current model yields also comparable but slightly smaller coordination numbers than the nonpolarizable model for alkali ions of Lee and Rasaiah.[126] Though the current model may be

expected to yield more accurate gas-phase properties for the small alkali ions, such consistency between the monohydrate properties and a unique absolute scale of hydration free energy, from polarizable and nonpolarizable models, suggests that it arises from a robust constraint in these systems.

4.3.2. Halide Ions. Figure 8 presents the RDFs of oxygen and hydrogen with respect to the halide ions. It shows clearly that the anions are coordinated by hydrogen atoms. From the positions of the first peak of the g_{IO} distribution and first and second peaks of the g_{IH} distribution, it can be seen that each water molecule provides a single coordinating hydrogen, whereas the second hydrogen populates a second maximum in g_{IH} further apart.

The coordination numbers of the halide ions are remarkably similar across the series (see Table 9). Although the positions of the first oxygen-coordination peak vary from 2.69 Å for fluoride to 3.49 Å for iodide (corresponding to an increase of 0.80 Å in the hydration radius), the larger coordination shell allows only one additional water molecule to insert ($N_c = 5.74$ for fluoride and 6.70 for iodide). In comparison, sodium has a coordination number of 5.67 for $r_{min1} = 2.37$ Å while cesium has $N_c = 9.55$ for r_{min1} only 0.78 Å longer. This might reflect the difficulty to create a compact hydration shell around anions.

Fluoride has $N_c = 5.74$ and chloride has $N_c = 6.50$, in agreement with most of the theoretical estimates and within the broad experimental range (see Table 2 of ref 127 and Table 8 of ref 128 and references therein). The QM/MM simulations of Tongraar and Rode[127] give 4.6 for fluoride and 5.6 for chloride, but their pure MM simulations (using a pairwise-additive force field) give both ions comparable coordination numbers (5.8 and 5.9, respectively). The position of the first oxygen-coordination peak of fluoride (2.69 Å) is comparable to most results from the literature (see ref 127 and ref 128), but that of chloride (3.14 Å) is relatively short: distances between 3.2 and 3.3 Å are more commonly obtained.[127,128]

For bromide, the first oxygen-coordination peak is at 3.27 Å and produces a coordination number $N_c = 6.59$. It is shorter than the data from Table 8 of ref 128 and the results of Merkling et al.[129] for the POT_2 model[55] (3.44 ± 0.07 Å and $N_c = 6 \pm 0.5$) but comparable to the CP results of Raugei and Klein[130] (3.26 Å and $N_c = 6.3$). The AH/SWM4-DP model predicts an oxygen coordination of 6.70 for iodide. Photoelectron spectroscopy suggests an optimal coordination of 6,[131] but this result could be tainted by the fact that iodide strongly prefers the surface of small water clusters.[52] In comparison, Ignaczak et al.[128] obtain $N_c = 9.1$ from Monte Carlo simulations with a pairwise-additive potential.

5. Conclusion

The hydration of alkali and halide was characterized using computer simulations based on an atomic model and a potential function incorporating the influence of induced polarization. The parameters of the potential function were systematically varied, and the properties of the model were evaluated. This procedure revealed that a unique model can be constructed that is simultaneously consistent with the energies and geometries of the monohydrates as well as the bulk solvation free energies. For this model, the solvation free energies of all neutral pairs of ions and the free energy differences between ions of like signs correspond nearly exactly to the experimental values. According to the model, the absolute scale corresponds to an hydration free energy of $\Delta G^{intr}_{hydr}(H^+) \simeq -247$ kcal/mol. In this regard, Figure 2 serves as a warning about the interpretation of calculations and measurements of hydration free energies. Calculations combining implicit and explicit representations of the solvent may create an artificial interface whose interaction with the ionic charge should be accounted for. This applies as well to the finite clusters and to the quasi-chemical approach. For the spherical solvent boundary potential (SSBP),[33] this interface potential was found to be almost identical to the air/water interface, and the calculated free energies were interpreted accordingly, that is, as ΔG^{real}_{hydr}. Given that the air/water potential is a difficult quantity to measure,[19] it becomes important to distinguish between the ΔG^{real}_{hydr} obtained from a simulation that reproduces or mimicks the interaction with the air/water interface, and the ΔG^{intr}_{hydr} obtained from a simulation that does not include any interface (e.g., that uses periodic boundary conditions). For those two values to be rigorously compared, the phase potential must be explicitly taken into consideration.

The model was also tested against the reproduction of zero-temperature hydrates. It is more successful for the microscopic hydration of alkali ions because the small cations are not significantly modifying the hydrogen-bonding structure of water. It is slightly less successful for halide hydration, probably because the first solvation shell of the halide ions undergoes severe distortions that are not representative of the bulk liquid water. This problem could arguably be tackled using a more robust representation of the hydrogen-bonding energetics, with slightly stronger hydrogen−hydrogen repulsion and perhaps explicit lone pairs instead of the unique "M" site of the SWM4-DP model (that was inspired by the TIP4P water model[34]). The precise shape of the oxygen−oxygen repulsive interaction could also be revisited. For that matter, a more complex water model could be tested against water hydrogen bonding within the first shell of a halide ion. That being said, these limitations do not seem to affect the properties of the anions in bulk water. Because the halogen ions are calibrated to produce hydration free energies thermodynamically consistent with those of the alkaline ions, some of the inaccuracies are probably "parametrized away."

Overall, the present approach seems to yield an acceptable compromise for the purpose of providing fully hydrated counterions in many-body simulations. The potential function has been used successfully by Archontis et al.[132] to model a solution of sodium and iodide. Nonetheless, it should be noted that, as the ion−ion LJ parameters generated from the Lorentz−Berthelot combination rule may not lead to quantitatively acccurate potentials to describe ion pairing in solution, accurate simulation of concentrated ionic solutions using the current model might require additional attention. Future work will examine these issues and pursue the development of calibrated polarizable models for ions in organic solvents following a similar approach.

Acknowledgment. This work was supported by Grant GM072558 from the National Institute of Health.

Supporting Information Available: Hydration free energy data and computations from the literature and complete refs 93 and 133. This material is available free of charge via the Internet at http://pubs.acs.org.

References and Notes

(1) Lybrand, T. P.; Kollman, P. A. *J. Chem. Phys.* **1985**, *83*, 2923.
(2) Sprik, M.; Klein, M. L.; Watanabe, K. *J. Phys. Chem.* **1990**, *94*, 6483.
(3) Dang, L. X.; Rice, J. E.; Caldwell, J.; Kollman, P. A. *J. Am. Chem. Soc.* **1991**, *113*, 2481.
(4) Roux, B. *Chem. Phys. Lett.* **1993**, *212*, 231.
(5) Stuart, S. J.; Berne, B. J. *J. Phys. Chem.* **1996**, *100*, 11934.

(6) Grossfield, A.; Ren, P.; Ponder, J. W. *J. Am. Chem. Soc.* **2003**, *125*, 15671.
(7) Roux, B.; Karplus, M. *J. Comput. Chem.* **1995**, *16*, 690.
(8) Latimer, W. M.; Pitzer, K. S.; Slansky, C. M. *J. Chem. Phys.* **1939**, *7*, 108.
(9) Randles, J. E. B. *Trans. Faraday Soc.* **1956**, *52*, 1573.
(10) Noyes, R. M. *J. Am. Chem. Soc.* **1962**, *84*, 513.
(11) Marcus, Y. *J. Chem. Soc., Faraday Trans. 1* **1986**, *82*, 233.
(12) Marcus, Y. *J. Chem. Soc., Faraday Trans. 1* **1987**, *83*, 339.
(13) Marcus, Y. *J. Chem. Soc., Faraday Trans. 1* **1987**, *83*.
(14) Gomer, R.; Tryson, G. *J. Chem. Phys.* **1977**, *66*, 4413.
(15) Klots, C. E. *J. Phys. Chem.* **1981**, *85*, 3585.
(16) Tissandier, M. D.; Cowen, K. A.; Feng, W. Y.; Gundlach, E.; Cohen, M. H.; Earhart, A. D.; Coe, J. V.; Tuttle, T. R., Jr. *J. Phys. Chem. A* **1998**, *102*, 7787.
(17) Schurhammer, R.; Engler, E.; Wipff, G. *J. Phys. Chem. B* **2001**, *105*, 10700.
(18) Llano, J.; Eriksson, L. A. *J. Chem. Phys.* **2002**, *117*, 10193.
(19) Paluch, M. *Adv. Colloid Interface Sci.* **2000**, *84*, 27.
(20) Asthagiri, D.; Pratt, L. R.; Ashbaugh, H. S. *J. Chem. Phys.* **2003**, *119*, 2702.
(21) Lamoureux, G.; MacKerell, A. D., Jr.; Roux, B. *J. Chem. Phys.* **2003**, *119*, 5185.
(22) Drude, P. *The Theory of Optics*; Longmans, Green, and Co.: New York, 1902.
(23) Saint-Martin, H.; Medina-Llanos, C.; Ortega-Blake, I. *J. Chem. Phys.* **1990**, *93*, 6448.
(24) de Leeuw, N. H.; Parker, S. C. *Phys. Rev. B* **1998**, *58*, 13901.
(25) Saint-Martin, H.; Hernández-Cobos, J.; Bernal-Uruchurtu, M. I.; Ortega-Blake, I.; Berendsen, H. J. C. *J. Chem. Phys.* **2000**, *113*, 10899.
(26) van Maaren, P. J.; van der Spoel, D. *J. Phys. Chem. B* **2001**, *105*, 2618.
(27) Yu, H.; Hansson, T.; van Gunsteren, W. F. *J. Chem. Phys.* **2003**, *118*, 221.
(28) Lamoureux, G.; Roux, B. *J. Chem. Phys.* **2003**, *119*, 3025.
(29) Stuart, S. J.; Berne, B. J. *J. Phys. Chem. A* **1999**, *103*, 10300.
(30) Lamoureux, G.; Harder, E.; Vorobyov, I. V.; Roux, B.; MacKerell, A. D., Jr. *Chem. Phys. Lett.* **2006**, *418*, 245.
(31) Allen, M. P.; Tildesley, D. J. *Computer Simulation of Liquids*; Clarendon Press: Oxford, 1987.
(32) Kumar, S.; Bouzida, D.; Swendsen, R. H.; Kollman, P. A.; Rosenberg, J. *J. Comput. Chem.* **1992**, *13*, 1011.
(33) Beglov, D.; Roux, B. *J. Chem. Phys.* **1994**, *100*, 9050.
(34) Jorgensen, W. L.; Chandrasekhar, J.; Madura, J. D.; Impey, R. W.; Klein, M. L. *J. Chem. Phys.* **1983**, *79*, 926.
(35) Feller, S. E.; Pastor, R. W.; Rojnuckarin, A.; Bogusz, S.; Brooks, B. R. *J. Phys. Chem.* **1996**, *100*, 17011.
(36) Hoover, W. G. *Phys. Rev. A* **1985**, *31*, 1695.
(37) Brooks, B. R.; Bruccoleri, R. E.; Olafson, B. D.; States, D. J.; Swaminathan, S.; Karplus, M. *J. Comput. Chem.* **1983**, *4*, 187.
(38) Darden, T.; York, D.; Pedersen, L. *J. Chem. Phys.* **1993**, *98*, 10089.
(39) Martyna, G. J.; Tobias, D. J.; Klein, M. L. *J. Chem. Phys.* **1994**, *101*, 4177.
(40) Rashin, A. A.; Topol, I. A.; Tawa, G. J.; Burt, S. K. *Chem. Phys. Lett.* **2001**, *335*, 327.
(41) Coker, H. *J. Phys. Chem.* **1976**, *80*, 2078.
(42) Mahan, G. D. *J. Chem. Phys.* **1982**, *76*, 493.
(43) Fowler, P. W.; Madden, P. A. *Phys. Rev. B* **1984**, *29*, 1035.
(44) Jemmer, P.; Fowler, P. W.; Wilson, M.; Madden, P. A. *J. Phys. Chem. A* **1998**, *102*, 8377.
(45) Jungwirth, P.; Tobias, D. J. *J. Phys. Chem. A* **2002**, *106*, 379.
(46) Valderrama, E.; Wheatley, R. J. *J. Comput. Chem.* **2003**, *24*, 2075.
(47) Coker, H. *J. Phys. Chem.* **1976**, *80*, 2084.
(48) Pyper, N. C.; Pike, C. G.; Edwards, P. P. *Mol. Phys.* **1992**, *76*, 353.
(49) Hättig, C.; Hess, B. A. *J. Chem. Phys.* **1998**, *108*, 3863.
(50) Perera, L.; Berkowitz, M. L. *J. Chem. Phys.* **1994**, *100*, 3085.
(51) Xantheas, S. S.; Dang, L. X. *J. Phys. Chem.* **1996**, *100*, 3989.
(52) Jungwirth, P.; Tobias, D. J. *J. Phys. Chem. B* **2002**, *106*, 6361.
(53) Markovich, G.; Perera, L.; Berkowitz, M. L.; Cheshnovsky, O. *J. Chem. Phys.* **1996**, *105*, 2675.
(54) Dang, L. X. *J. Phys. Chem. B* **2002**, *106*, 10388.
(55) Ayala, R.; Martínez, J. M.; Pappalardo, R. R.; Saint-Martin, H.; Ortega-Blake, I.; Marcos, E. S. *J. Chem. Phys.* **2002**, *117*, 10512.
(56) Nguyen, T. N. V.; Peslherbe, G. H. *J. Phys. Chem. A* **2003**, *107*, 1540.
(57) Nellin, C.; Roos, B. O.; Sadlej, A. J.; Siegbahn, P. E. M. *J. Chem. Phys.* **1982**, *77*, 3607.
(58) Kello, V.; Roos, B. O.; Sadlej, A. J. *Theor. Chim. Acta* **1988**, *74*, 185.
(59) Fowler, P. W.; Tole, P. *J. Chem. Soc., Faraday Trans.* **1990**, *86*, 1019.
(60) Mahan, G. D. *Phys. Rev. A* **1980**, *22*, 1780.
(61) Carignano, M. A.; Karlström, G.; Linse, P. *J. Phys. Chem. B* **1997**, *101*, 1142.
(62) Džidić, I.; Kebarle, P. *J. Phys. Chem.* **1970**, *74*, 1466.
(63) Hiraoka, K.; Mizuse, S.; Yamabe, S. *J. Phys. Chem.* **1988**, *92*, 3943.
(64) Rodgers, M. T.; Armentrout, P. B. *J. Phys. Chem. A* **1997**, *101*, 1238.
(65) Feller, D.; Glendening, E. D.; Kendall, R. A.; Peterson, K. A. *J. Chem. Phys.* **1994**, *100*, 4981.
(66) Glendening, E. D.; Feller, D. *J. Phys. Chem.* **1995**, *99*, 3060.
(67) Kim, J.; Lee, S.; Cho, S. J.; Mhin, B. J.; Kim, K. S. *J. Chem. Phys.* **1995**, *102*, 839.
(68) Bene, J. E. D. *J. Phys. Chem.* **1996**, *100*, 6284.
(69) Hashimoto, K.; Kamimoto, T. *J. Am. Chem. Soc.* **1998**, *120*, 3560.
(70) Lee, H. M.; Kim, J.; Lee, S.; Mhin, B. J.; Kim, K. S. *J. Chem. Phys.* **1999**, *111*, 3995.
(71) El-Nahas, A. M.; Hirao, K. *J. Phys. Chem. A* **2000**, *104*, 138.
(72) Borodin, O.; Bell, R. L.; Li, Y.; Bedrov, D.; Smith, G. D. *Chem. Phys. Lett.* **2001**, *336*, 292.
(73) Kim, J.; Lee, H. M.; Suh, S. B.; Majumdat, D.; Kim, K. S. *J. Chem. Phys.* **2000**, *113*, 5259.
(74) Xantheas, S. S. *J. Phys. Chem.* **1996**, *100*, 9703.
(75) Huheey, J. E.; Keiter, E. A.; Keiter, R. L. *Inorganic Chemistry: Principles of Structure and Reactivity*, 4th ed.; Harper Collins: New York,-1993.
(76) Zhan, C.-G.; Dixon, D. A. *J. Phys. Chem. A* **2001**, *105*, 11534.
(77) Zhan, C.-G.; Dixon, D. A. *J. Phys. Chem. A* **2004**, *108*, 2020.
(78) Brodskaya, E. N.; Zakharov, V. V. *J. Chem. Phys.* **1995**, *102*, 4595.
(79) Stillinger, F. H.; Rahman, A. *J. Chem. Phys.* **1974**, *60*, 1545.
(80) Sokhan, V. P.; Tildesley, D. J. *Mol. Phys.* **1997**, *92*, 625.
(81) Berendsen, H. J. C.; Grigera, J. R.; Straatsma, T. P. *J. Phys. Chem.* **1987**, *91*, 6269.
(82) Rick, S. W.; Stuart, S. J.; Berne, B. J. *J. Chem. Phys.* **1994**, *101*, 6141.
(83) Dang, L. X.; Chang, T.-M. *J. Phys. Chem. B* **2002**, *106*, 235.
(84) Dang, L. X.; Chang, T.-M. *J. Chem. Phys.* **1997**, *106*, 8149.
(85) Ashbaugh, H. S. *J. Phys. Chem. B* **2000**, *104*, 7235.
(86) Hummer, G.; Pratt, L. R.; García, A. E. *J. Chem. Phys.* **1997**, *107*, 9275.
(87) Coe, J. V. *J. Phys. Chem. A* **1997**, *101*, 2055.
(88) Tuttle, T. R.; Malaxos, S.; Coe, J. V. *J. Phys. Chem. A* **2002**, *106*, 925.
(89) Honeycutt, A. J.; Saykally, R. J. *Science* **2003**, *299*, 1329.
(90) Kaupp, M.; v. R. Schleyer, P. *J. Phys. Chem.* **1992**, *96*, 7316.
(91) Feller, D. *J. Phys. Chem. A* **1997**, *101*, 2723.
(92) Ayotte, P.; Nielsen, S. B.; Weddle, G. H.; Johnson, M. A.; Xantheas, S. S. *J. Phys. Chem. A* **1999**, *103*, 10665.
(93) Frisch, M. J.; Trucks, G. W.; Schlegel, H. B.; Scuseria, G. E.; Robb, M. A.; Cheeseman, J. R.; Zakrzewski, V. G.; Montgomery, J. A., Jr.; Stratmann, R. E.; Burant, J. C.; Dapprich, S.; Millam, J. M.; Daniels, A. D.; Kudin, K. N.; Strain, M. C.; Farkas, O.; Tomasi, J.; Barone, V.; Cossi, M.; Cammi, R.; Mennucci, B.; Pomelli, C.; Adamo, C.; Clifford, S.; Ochterski, J.; Petersson, G. A.; Ayala, P. Y.; Cui, Q.; Morokuma, K.; Malick, D. K.; Rabuck, A. D.; Raghavachari, K.; Foresman, J. B.; Cioslowski, J.; Ortiz, J. V.; Stefanov, B. B.; Liu, G.; Liashenko, A.; Piskorz, P.; Komaromi, I.; Gomperts, R.; Martin, R. L.; Fox, D. J.; Keith, T.; Al-Laham, M. A.; Peng, C. Y.; Nanayakkara, A.; Gonzalez, C.; Challacombe, M.; Gill, P. M. W.; Johnson, B. G.; Chen, W.; Wong, M. W.; Andres, J. L.; Head-Gordon, M.; Replogle, E. S.; Pople, J. A. *Gaussian 98*, revision A.9; Gaussian, Inc.: Pittsburgh, PA, 1998.
(94) Masamura, M. *J. Phys. Chem. A* **2002**, *106*, 8925.
(95) Lee, H. M.; Kim, K. S. *J. Chem. Phys.* **2001**, *114*, 4461.
(96) Bryce, R. A.; Vincent, M. A.; Malcolm, N. O. J.; Hillier, I. H.; Burton, N. A. *J. Chem. Phys.* **1998**, *109*, 3077.
(97) Robertson, W. H.; Diken, E. G.; Price, E. A.; Shin, J.-W.; Johnson, M. A. *Science* **2003**, *299*, 1367.
(98) Duan, Z.; Zhang, Z. *Mol. Phys.* **2003**, *101*, 1501.
(99) Combariza, J. E.; Kestner, N. R. *J. Phys. Chem.* **1994**, *98*, 3513.
(100) Combariza, J. E.; Kestner, N. R.; Jortner, J. *J. Chem. Phys.* **1994**, *100*, 2851.
(101) Rempe, S. B.; Pratt, L. R.; Hummer, G.; Kress, J. D.; Martin, R. L.; Recondo, A. *J. Am. Chem. Soc.* **2000**, *122*, 966.
(102) Lyubartsev, A. P.; Laasonen, K.; Laaksonen, A. *J. Chem. Phys.* **2001**, *114*, 3120.
(103) Loeffler, H. H.; Rode, B. M. *J. Chem. Phys.* **2002**, *117*, 110.
(104) Spångberg, D.; Rey, R.; Hynes, J. T.; Hermansson, K. *J. Phys. Chem. B* **2003**, *107*, 4470.
(105) Loeffler, H. H. *J. Comput. Chem.* **2003**, *24*, 1232.
(106) Tongraar, A.; Liedl, K. R.; Rode, B. M. *J. Phys. Chem. A* **1998**, *102*, 10340.
(107) White, J. A.; Schewegler, E.; Galli, G.; Gygi, F. *J. Chem. Phys.* **2000**, *113*, 4668.
(108) Carrillo-Tripp, M.; Saint-Martin, H.; Ortega-Blake, I. *J. Chem. Phys.* **2003**, *118*, 7062.

(109) Rempe, S. B.; Pratt, L. R. *Fluid Phase Equilibria* **2000**, *183*, 121.
(110) Ramaniah, L. M.; Bernasconi, M.; Parrinello, M. *J. Chem. Phys.* **1999**, *111*, 1587.
(111) Palinkas, G.; Radnai, T.; Hajdu, F. *Z. Naturforsch. A: Phys. Sci.* **1980**, *35*, 107.
(112) Neilson, G. W.; Skipper, N. *Chem. Phys. Lett.* **1985**, *114*, 35.
(113) Chuev, G. N.; Fedorov, M. V. *Phys. Rev. E* **2003**, *68*, 1.
(114) Marcus, Y. *Chem. Rev.* **1988**, *88*, 1475.
(115) Hofer, T. S.; Randolf, B. R.; Rode, B. M. *J. Comput. Chem.* **2005**, *26*, 949.
(116) Schwenk, C. F.; Hofer, T. S.; Rode, B. M. *J. Phys. Chem. A* **2004**, *108*, 1509.
(117) Kubozono, Y.; Hirano, A.; Maeda, H.; Kashino, S.; Emura, S.; Ishida, H. *Z. Naturforsch., A: Phys. Sci.* **1994**, *49*, 727.
(118) Fulton, J. L.; Pfund, D. M.; Wallen, S. L.; Newville, M.; Stern, E. A.; Ma, Y. J. *J. Chem. Phys.* **1996**, *105*, 2161.
(119) Filipponi, A.; Panfilis, S. D.; Oliva, C.; Ricci, M. A.; D'Angelo, P.; Bowron, D. T. *Phys. Rev. Lett.* **2003**, *91*, 165505.
(120) Enderby, J. E. *Chem. Soc. Rev.* **1995**, *24*, 159.
(121) Smirnov, P. R.; Trostin, V. N. *Zh. Fiz. Khim.* **1995**, *69*, 1218.
(122) Skipper, N. T.; Neilson, G. W. *J. Phys.: Condens. Matter* **1989**, *1*, 4141.
(123) Guàrdia, E.; Padró, J. A. *J. Phys. Chem.* **1990**, *94*, 6049.
(124) Guymon, C. G.; Hunsaker, M. L.; Harb, J. N.; Henderson, D.; Rowley, R. L. *J. Chem. Phys.* **2003**, *118*, 10195.
(125) Åqvist, J. *J. Phys. Chem.* **1990**, *94*, 8021.
(126) Lee, S. H.; Rasaiah, J. C. *J. Phys. Chem.* **1996**, *100*, 1420.
(127) Tongraar, A.; Rode, B. M. *Phys. Chem. Chem. Phys.* **2003**, *5*, 357.
(128) Ignaczak, A.; Gomes, J. A. N. F.; Cordeiro, M. N. D. S. *Electrochim. Acta* **1999**, *45*, 659.
(129) Merkling, P. J.; Ayala, R.; Martínez, J. M.; Pappalardo, R. R.; Marcos, E. S. *J. Chem. Phys.* **2003**, *119*, 6647.
(130) Raugei, S.; Klein, M. L. *J. Am. Chem. Soc.* **2001**, *123*, 9484.
(131) Markovich, G.; Giniger, R.; Levin, M.; Cheshnovsky, O. *J. Chem. Phys.* **1991**, *95*, 9416.
(132) Archontis, G.; Leontidis, E.; Andreou, G. *J. Phys. Chem. B* **2005**, *109*, 17957.
(133) MacKerell, A. D., Jr.; Bashford, D.; Bellott, M.; Dunbrack, R. L., Jr.; Evanseck, J. D.; Field, M. J.; Fischer, S.; Gao, J.; Guo, H.; Ha, S.; Joseph-McCarthy, D.; Kuchnir, L.; Kuczera, K.; Lau, F. T. K.; Mattos, C.; Michnick, S.; Ngo, T.; Nguyen, D. T.; Prodhom, M.; Reiher, W. E., III; Roux, B.; Schlenkrich, M.; Smith, J. C.; Stote, R.; Straub, J.; Watanabe, M.; Wiórkiewicz-Kuczera, J.; Yin, D.; Karplus, M. *J. Phys. Chem. B* **1998**, *102*, 3586.